Supplementary Information

Size-Matching Overrides the Electronic Preference of Cation-π Interactions in a Deep Cavitand

Qi-Qi Wang,[ab] Wen-Kai Yang[b] and Yang Yu[b]

[a] Department of Physics, College of Sciences, Shanghai University, Shanghai, 200444, China

[b] Center for Supramolecular Chemistry & Catalysis and Department of Chemistry, College of Science, Shanghai University, 200444, China

Content

1. General information

1) Materials

Reagents were purchased from companies such as Macklin Reagent, Energy Chemical and Sinopharm Chemical Reagent, and used without further purification unless otherwise stated. The cavitand **H** (with pyridinium groups at both the upper and lower rims) and cavitand **H'** (with neutral upper rim and pyridinium groups at the lower rim) were synthesized according to literature methods.[1,2] 4-heptylpyridine (P7) and 4-octylpyridine (P8) were synthesized according to literature methods.[3]

2) Methods

I. Nuclear magnetic resonance (NMR)

^{1}H NMR and 2D ^{1}H-^{1}H NOESY spectra were recorded on a Bruker AVANCE III HD 600 MHz instrument at 298 K. Deuterated reagents were used with tetramethylsilane (TMS) as an internal standard. The chemical shifts of the deuterated solvent peaks are referenced as follows: D_2O δ = 4.79 ppm, CD_3OD δ = 3.31 ppm.

The preparation for the experiments of guests with hosts were carried out as follows: first, prepare the **H** solution (500 μL, 1 mmol/L in D_2O) in the NMR tube. Then add the guest solution (10 μL, 50 mmol/L in CD_3OD) and followed by ultrasonication for 4 hours before ^{1}H NMR and 2D ^{1}H-^{1}H NOESY testing. The concentration ratio is [**H**]: [guest] = 1:1. The pD of all NMR samples was maintained within 6.5~7.0 before and after guest addition.

The preparation for the experiments of different guests with host were carried out as follows: first, prepare the **H** solution (500 μL, 1 mmol/L in D_2O) in the NMR tube. Then add the mixture of guest A (10 μL, 50 mmol/L in CD_3OD) and guest B (10 μL, 50 mmol/L in CD_3OD) solutions and followed by ultrasonication for 4 hours before ^{1}H NMR testing. The concentration ratio is [**H**]: [guest A]: [guest B] = 1:1:1.

The preparation for the competition experiments of different hosts with guest were carried out as follows: first, prepare the **H** solution (250 μL, 2 mmol/L in D_2O) and the **H'** solution (250 μL, 2 mmol/L in D_2O) in the NMR tube and shake it to mix the solutions thoroughly. Then add the guest solution (2 μL, 50 mmol/L in CD_3OD) and followed by ultrasonication for 4 hours before ^{1}H NMR testing. The concentration ratio is [**H**]: [**H'**]: [guest] = 1:1:0.2.

$\Delta\delta$ value is $\Delta\delta = \delta_{bound} - \delta_{free}$.

II. Isothermal titration calorimetry (ITC)

ITC experiments were performed using a TA NANO ITC instrument. The sample cell was loaded with 0.17 mL of the **H** solution (0.5 mmol/L, pH 6.5~7) in 5% (v/v) MeOH/water at 25 °C, and the syringe was filled with 50 μL of guest solution (5 mmol/L) in 5% (v/v) MeOH/water. The pH of the complex solution remains within 6-8 for all guests. The titration procedure consisted of 25 injections of 2 μL each of the guest solution, with an interval of 360s between injections. All data were corrected by subtracting the heat of dilution obtained from titrating guest into 5% (v/v) MeOH/water. The data were fitted using the 1:1 "Independent" binding model. The good agreement between the fitted curves and the experimental data (as evidenced by random residuals) supports the validity of this 1:1 binding model. The reported binding constants in main text represent the average of three independent experiments. Residuals were randomly distributed around zero without systematic trends, confirming that the applied binding model adequately describes the experimental data.

The reliability of the fitted binding constants was evaluated using the *c* value,[4-6] defined as:

$$c = \frac{[Titrand]}{K_D} = [Titrand] \cdot K_a$$

where [*Titrand*] is the initial concentration in the cell, here is 0.5 mmol/L (5×10^{-4} mol/L), and K_a is the binding constant. The *c* value determines the shape of the titration curve and the stability of the nonlinear regression: when $5 < c < 500$, the curve exhibits a clear sigmoidal shape, and the fitted parameters are robust against experimental noise.

Accordingly, for each key complex, we calculated the *c* value and the relative standard deviation (RSD) from triplicate measurements to assess the reliability of the binding parameters.

2. Recognition behaviors of 4-alkylpyridines by cavitand H

For P5-P8, the group located deepest within the cavity is a CH_2 unit rather than the terminal CH_3 group (Table S1), establishing folded alkyl tail conformation. For P5, the chemical shift ($\Delta\delta$) value of the terminal CH_3 group is −3.66 ppm, close to that of the adjacent methylene C4 at −3.88 ppm, indicating a relatively low degree of folding. For P6-P8, the terminal CH_3 group exhibits more pronounced upward folded, with the $\Delta\delta$ values (ranging from −2.26 to −0.81 ppm) less negative than that of the α-CH_2 group connected to the pyridine (about −3.50 ppm), indicating that the terminal CH_3 is positioned closest to the cavity opening.

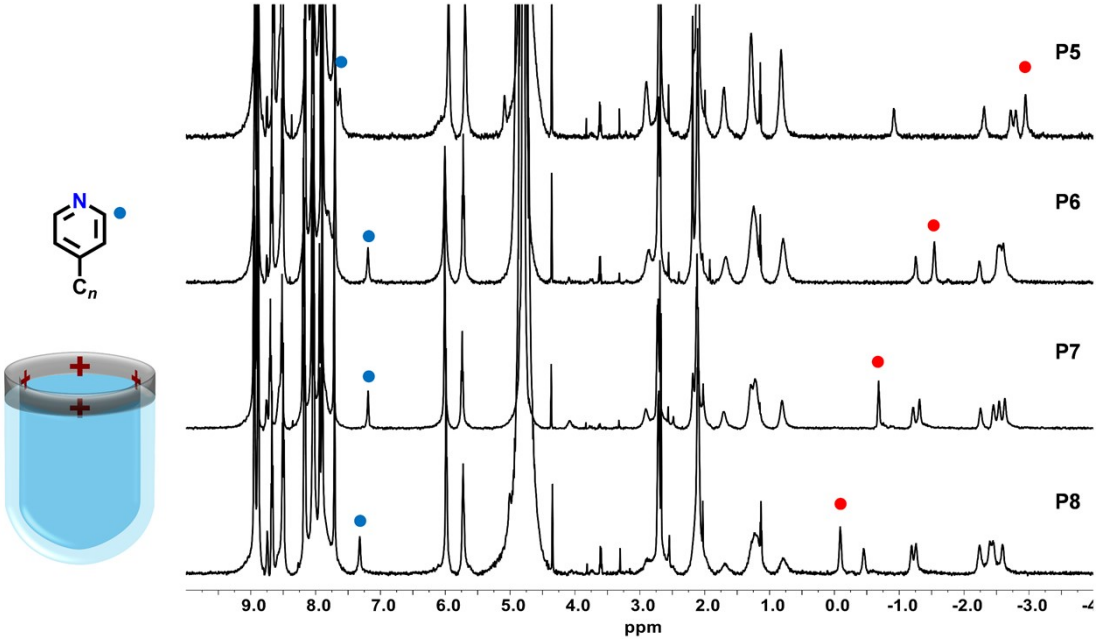

Fig. S1 ^{1}H NMR (600 MHz, D_2O, 298 K) spectra of **H** bound to 4-alkylpyridine guests. The blue dots represent the positions of the α-CH protons (P_α) adjacent to the pyridine *N*, and the red dots correspond to the terminal CH_3 groups of guests.

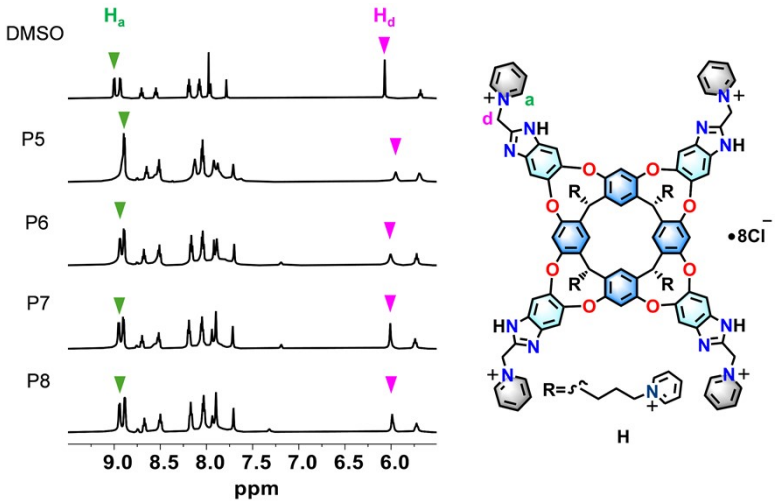

Fig. S2 Partial ^{1}H NMR (600 MHz, D_2O, 298 K) spectra (5.5 to 9.5 ppm) of **H** bound to DMSO and 4-alkylpyridine guests. The green and pink triangles indicate the H_a and H_d positions of **H** after bound to 4-alkylpyridine guests.

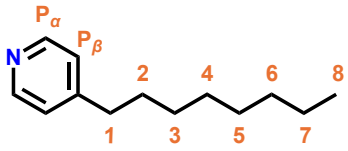

Fig. S3 The structure of P8.

Table S1. Δδ values of alkyl chains for 4-alkylpyridine guests upon bound to **H**

G@**H** / Δδ/ppm / C_n	P5 @**H**	P6 @**H**	P7 @**H**	P8 @**H**
P_α	−0.62	−1.06	−1.06	−0.93
1	−3.23	−3.58	−3.52	−3.57
2	−3.69	−3.61	−3.63	−3.62
3	−3.82	−3.64	−3.73	−3.68
4	−3.88	−3.70	−3.63	−3.54
5	−3.66	−3.62	−3.54	−3.49
6		−2.26	−2.40	−2.27
7			−1.40	−1.54
8				−0.81

Table S2 Δδ values of alkyl chains for alkylbenzene guests upon bound to **H**[1]

G@**H** / Δδ/ppm / C_n	B5 @**H**	B6 @**H**	B7 @**H**	B8 @**H**
1	−2.86	−2.34	−2.45	−2.42
2	−3.37	−2.89	−2.83	−2.77
3	−3.88	−3.39	−3.14	−2.94
4	−4.20	−3.69	−3.34	−3.17
5	−4.43	−3.97	−3.58	−3.33
6		−3.77	−3.34	−3.06
7			−2.78	−2.59
8				−2.06

Table S3. The Δδ values for H_a and H_d of **H** bound to 4-alkylpyridine guests

H@G / Δδ/ppm / C_n	**H**@P5	**H**@P6	**H**@P7	**H**@P8
H_a	−0.11	−0.07	−0.05	−0.06
H_d	−0.12	−0.06	−0.06	−0.09

Table S4. The Δδ values for H_a and H_d of **H** bound to alkylbenzene guests[1]

H@G / Δδ/ppm / C_n	**H**@B5	**H**@B6	**H**@B7	**H**@B8
H_a	−0.22	−0.22	−0.18	−0.18
H_d	−0.38	−0.21	−0.27	−0.25

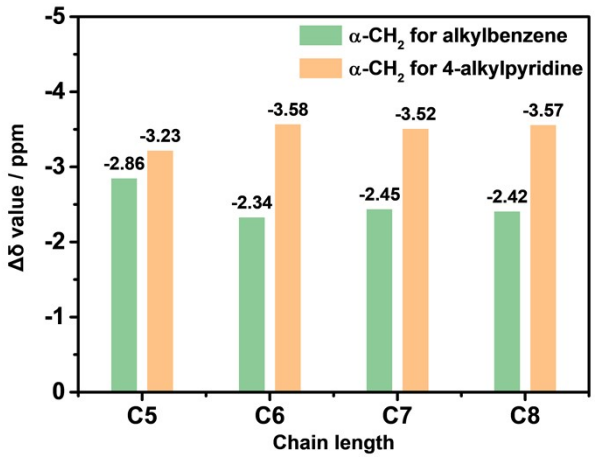

Fig. S4 Bar chart showing the variation of Δδ values for α-CH_2 groups of 4-alkylpyridines and alkylbenzenes (n = 5-8) within **H**.

The alkyl chains of P6 adopt a folded conformation within the cavity of the cationic cavitand **H**. The 2D ^{1}H-^{1}H NOESY spectrum (Fig. S5) indicate correlations among the various groups of P6, as detailed below: C1↔C3, C1↔C4, C1↔C5; C2↔C3, C2↔C4, C2↔C5, C2↔C6; C3↔C4, C3↔C5; C4↔C5, C4↔C6; C5↔C6. Meanwhile, a weak correlation is also observed between the terminal CH_3 group C6 of P6 and H_d on the upper rim of the cavitand **H** (Fig. S6).

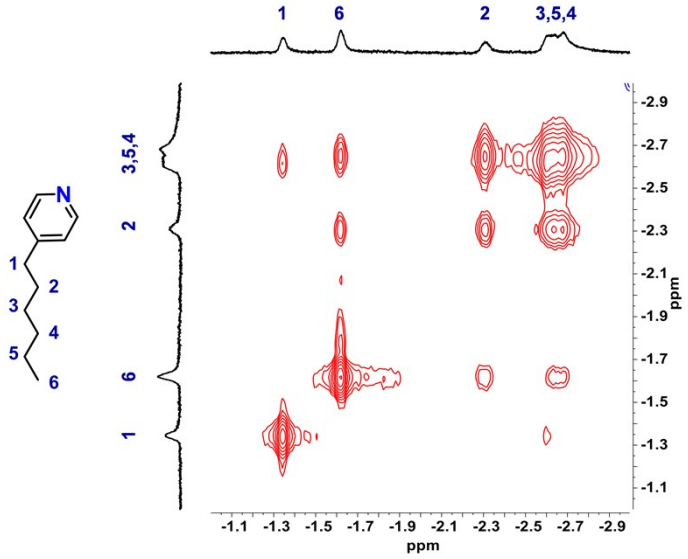

Fig. S5 Partial 2D ^{1}H-^{1}H NOESY NMR (600 MHz, D_2O, 298 K) spectrum (−3.0 to −1 ppm) of **H** bound with P6.

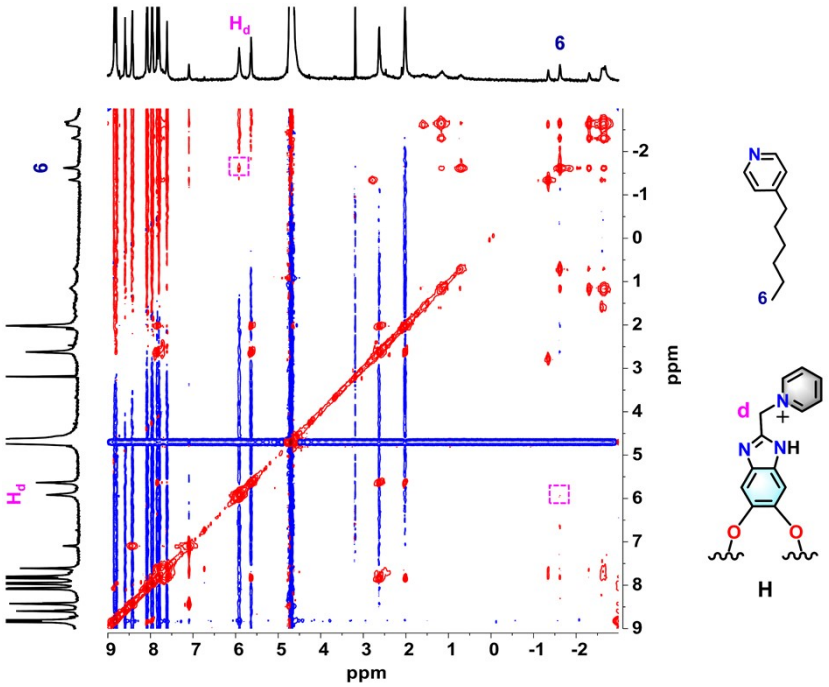

Fig. S6 2D ^{1}H-^{1}H NOESY NMR spectrum (600 MHz, D_2O, 298 K) of **H** bound to P6.

P7 also adopt a folded conformation within the cavity of the cationic cavitand **H**. The 2D ^{1}H-^{1}H NOESY spectrum (Fig. S7) indicate correlations among the various groups of P7, as detailed below: C1↔C2, C1↔C3, C1↔C5, C1↔C7; C2↔C3, C2↔C5; C3↔C4, C3↔C5; C4↔C5, C4↔C6. Meanwhile, a weak correlation is also observed between the terminal CH_3 group C7 of P7 and H_d on the upper rim of the cavitand **H** (Fig. S8).

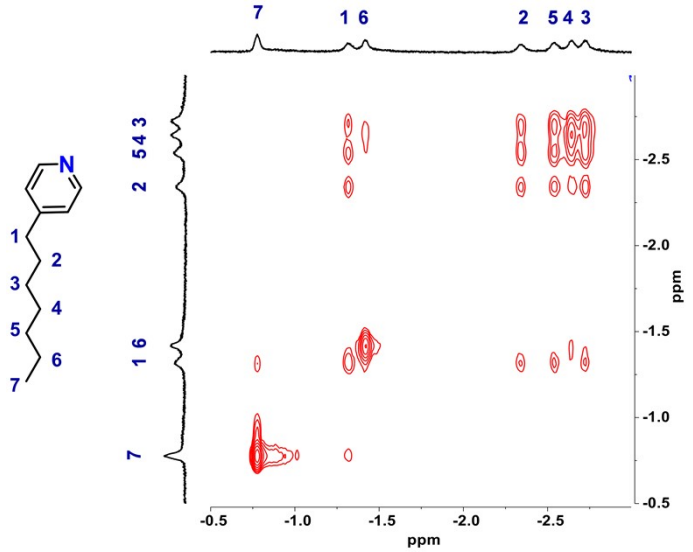

Fig. S7 Partial 2D ^{1}H-^{1}H NOESY NMR (600 MHz, D_2O, 298 K) spectrum (−3.0 to −0.5 ppm) of **H** bound to P7.

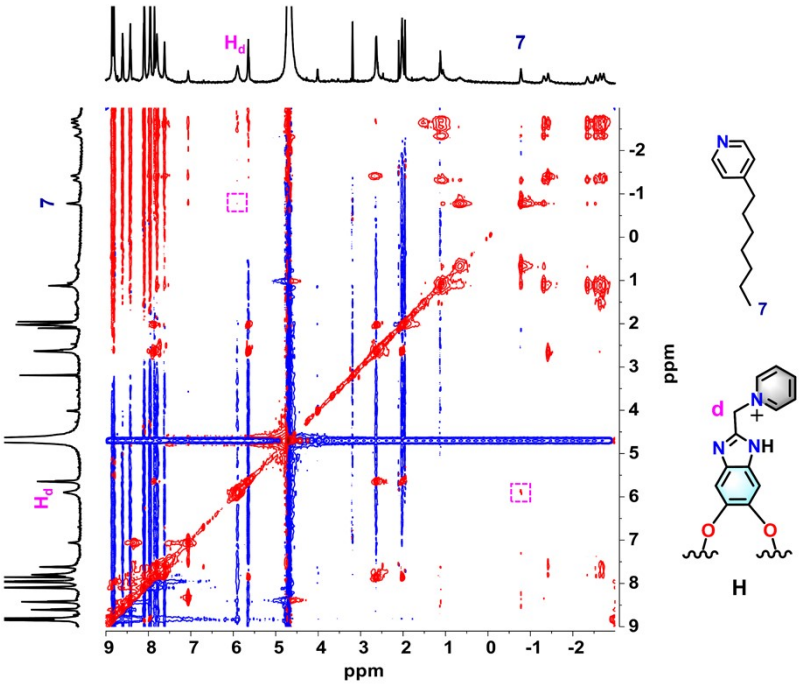

Fig. S8 2D ^{1}H-^{1}H NOESY NMR (600 MHz, D_2O, 298 K) spectrum of **H** bound to P7.

3. Competition experiments for alkylbenzene and 4-alkylpyridine

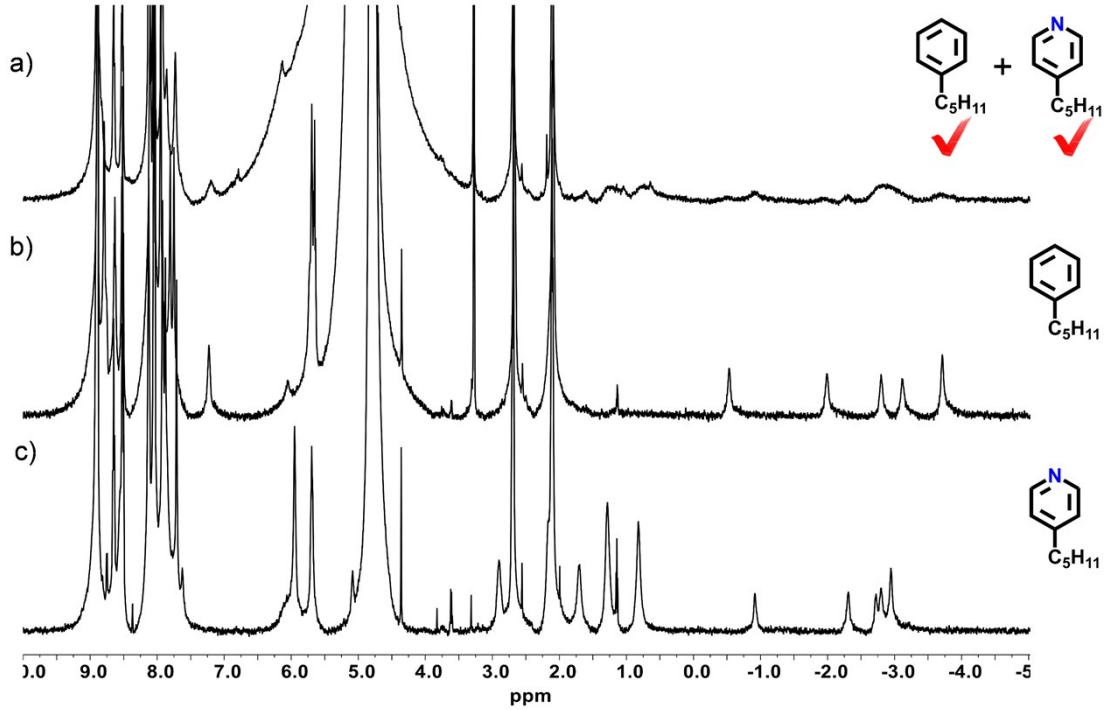

Fig. S9 ^{1}H NMR (600 MHz, D_2O, 298 K) spectra of a) B5, P5 and **H**, b) B5@**H**, c) P5@**H**. [**H**] = [B5] = [P5] = 1 mmol/L. The red checkmarks indicate the guests enter into the cavity of **H**.

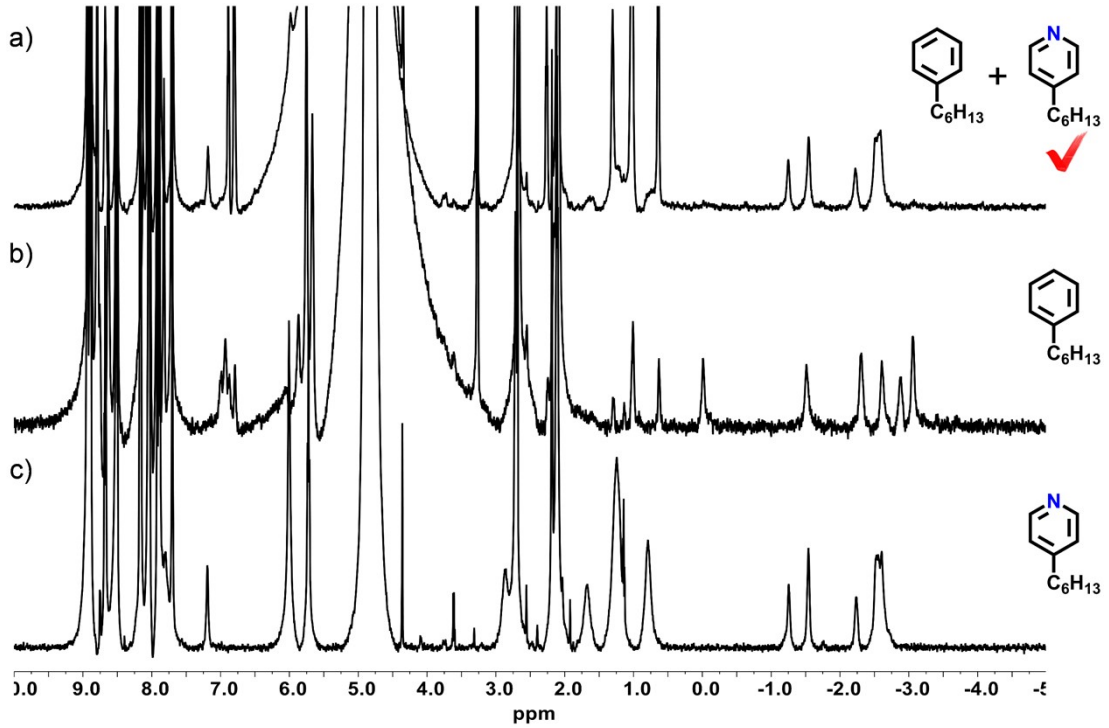

Fig. S10 ^{1}H NMR (600 MHz, D_2O, 298 K) spectra of a) B6, P6 and **H**, b) B6@**H**, c) P6@**H**. [**H**] = [B6] = [P6] = 1 mmol/L. The red checkmark indicates the guest enters into the cavity of **H**.

Two independent competition experiments for B6 vs. P6 both show exclusive encapsulation of P6 (Fig. S11), confirming the reproducibility of the selectivity.

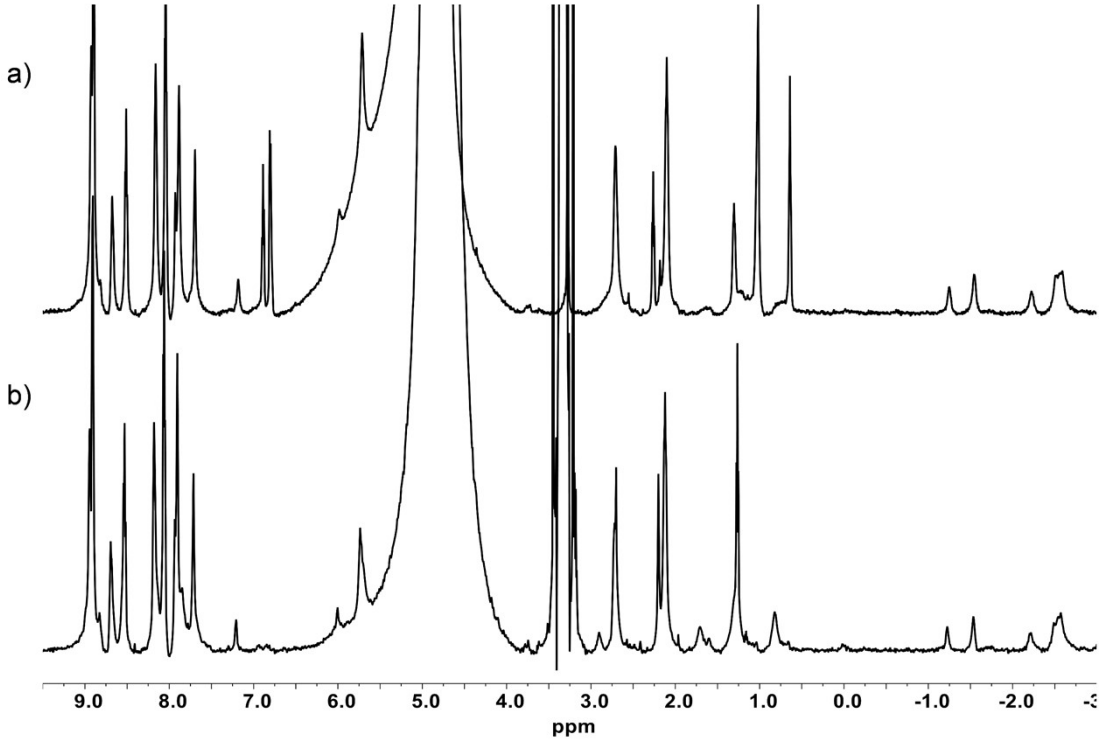

Fig. S11 ^{1}H NMR (600 MHz, D_2O, 298 K) spectra of two independent replicate competition experiments (a and b) of B6, P6 and **H**. [**H**] = [B6] = [P6] = 1 mmol/L.

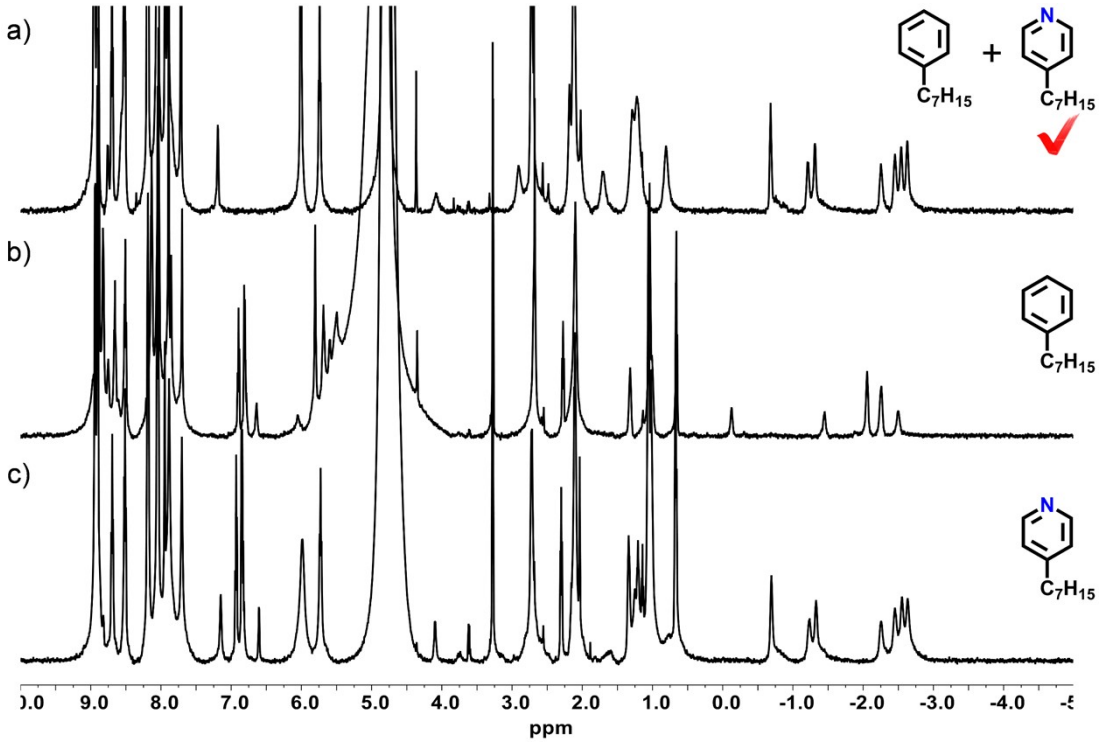

Fig. S12 ^{1}H NMR (600 MHz, D_2O, 298 K) spectra of a) B7, P7 and **H**, b) B7@**H**, c) P7@**H**. [**H**] = [B7] = [P7] = 1 mmol/L. The red checkmark indicates the guest enters into the cavity of **H**.

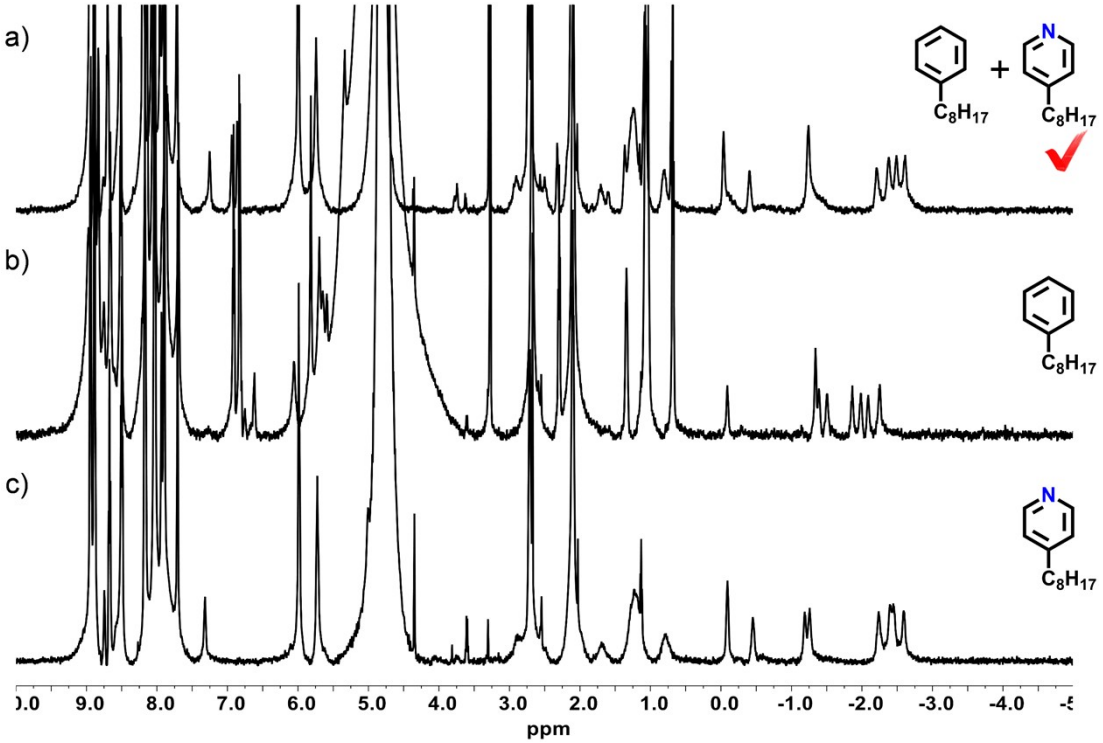

Fig. S13 ^{1}H NMR (600 MHz, D_2O, 298 K) spectra of a) B8, P8 and **H**, b) B8@**H**, c) P8@**H**. [**H**] = [B8] = [P8] = 1 mmol/L. The red checkmark indicates the guest enters into the cavity of **H**.

Based on the K_a value obtained from three independent experiments (Table S5), the c value was calculated to be 2.72. According to the literature[4-6], the K_a can be determined with reasonable reliability for titration curves that exhibit a clear sigmoidal shape and reach a saturation plateau. The titration curve shows a distinct inflection point and a clear terminal plateau, the fit residuals are randomly distributed between –2 and 1, and the RSD of K_a is 4.43%. Therefore, the binding constant for the B6@**H** complex is considered reliable.

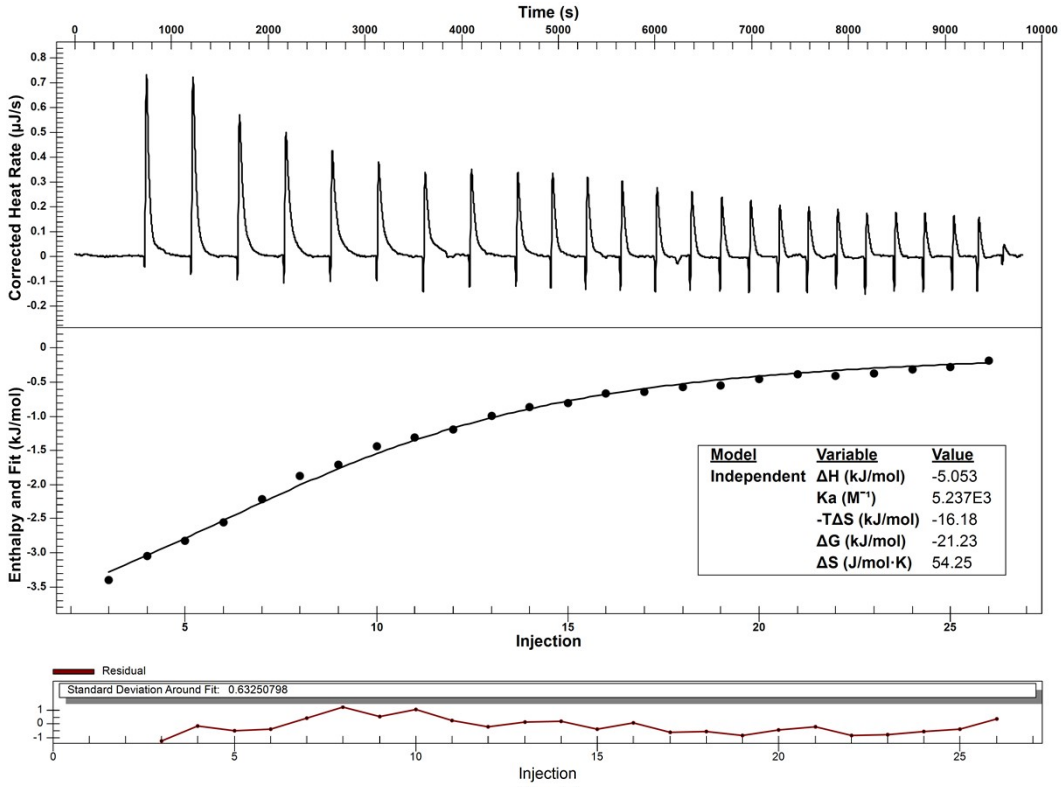
Time (s)
Corrected Heat Rate (µJ/s)
Enthalpy and Fit (kJ/mol)
Injection
Model Variable Value
Independent ΔH (kJ/mol) -5.053
Ka (M⁻¹) 5.237E3
-TΔS (kJ/mol) -16.18
ΔG (kJ/mol) -21.23
ΔS (J/mol·K) 54.25
Residual
Standard Deviation Around Fit: 0.63250798
Injection

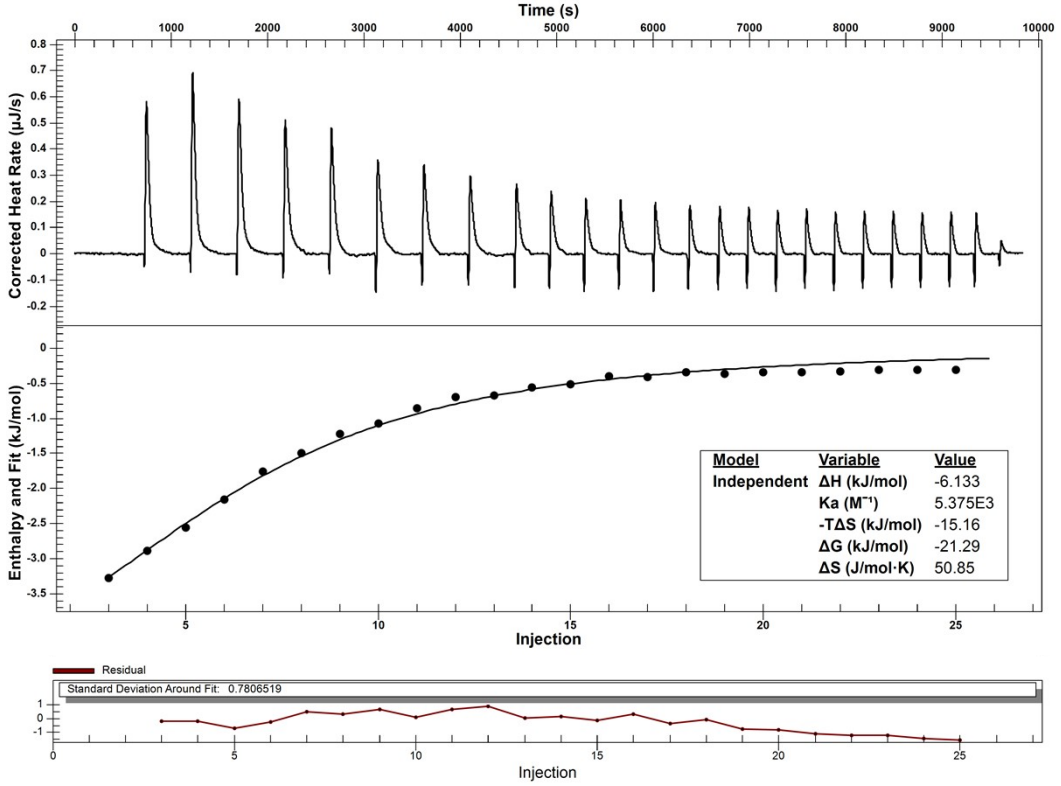
Time (s)
Corrected Heat Rate (µJ/s)
Enthalpy and Fit (kJ/mol)
Injection
Model Variable Value
Independent ΔH (kJ/mol) -6.133
Ka (M⁻¹) 5.375E3
-TΔS (kJ/mol) -15.16
ΔG (kJ/mol) -21.29
ΔS (J/mol·K) 50.85
Residual
Standard Deviation Around Fit: 0.7806519
Injection

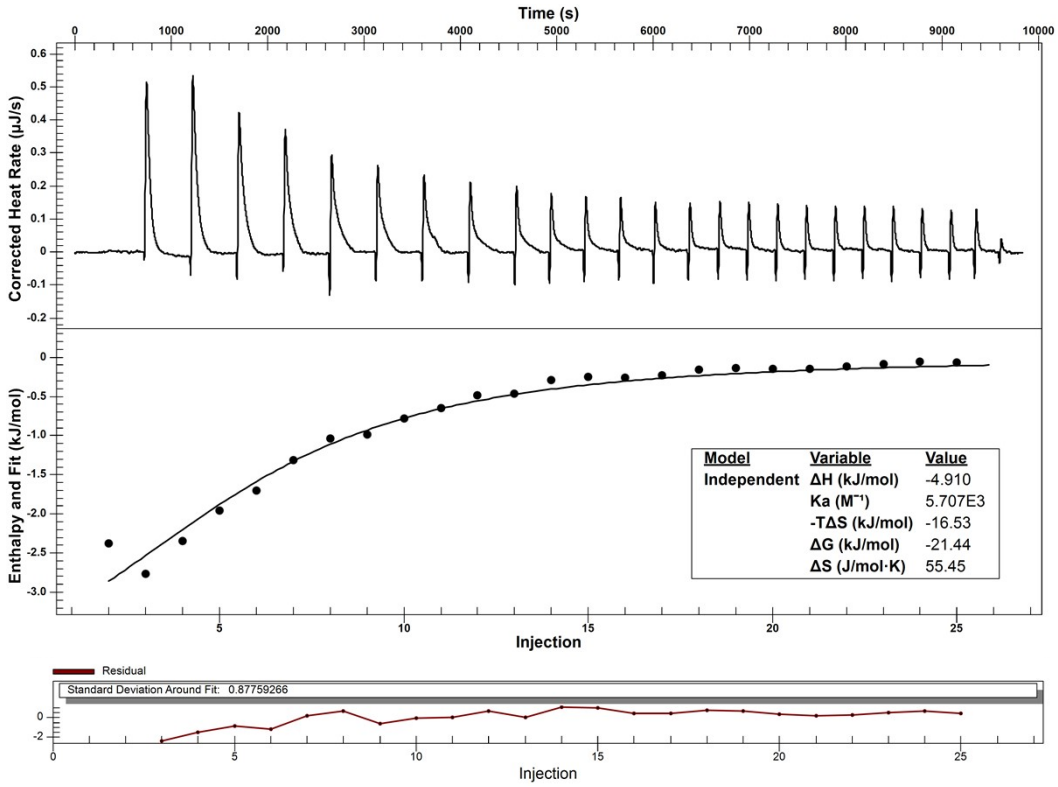

Fig. S14 Results from three independent ITC titrations of cavitand **H** (0.5 mmol/L) with B6 (5 mmol/L) in 5% (v/v) MeOH/water. The raw titration curves (top), the corresponding reaction heat obtained from the integration of each injection peak (middle), and residual plot of the fit (bottom).

Table S5. Triplicate ITC data for the B6@**H** complex

	1	2	3	Mean ± SD (K_a / M^{-1})	RSD / %
K (M^{-1})	5.24×10^3	5.38×10^3	5.71×10^3	$(5.44 \pm 0.24) \times 10^3$	4.43
ΔH (kJ/mol)	−5.05	−6.13	−4.91	−5.36 ± 0.67	12.5
ΔG (kJ/mol)	−21.23	−21.29	−21.44	−21.32 ± 0.11	0.51
ΔS (J/mol·K)	54.25	50.85	55.45	53.52 ± 2.39	4.46
Residual SD	0.63	0.78	0.88	-	-

Note: values are rounded to two decimal places

Based on the K_a value obtained from three independent experiments (Table S6), the c value was calculated to be 9.3. This value falls within the conventionally recommended range of 5-500, indicating favorable experimental conditions for reliable ITC fitting. The titration curve exhibits a clear sigmoidal shape with a distinct inflection point and a terminal plateau, the fit residuals are randomly distributed (within –2.5 to 2.5), and the RSD of K_a is 4.84%. Thus, the results are reliable.

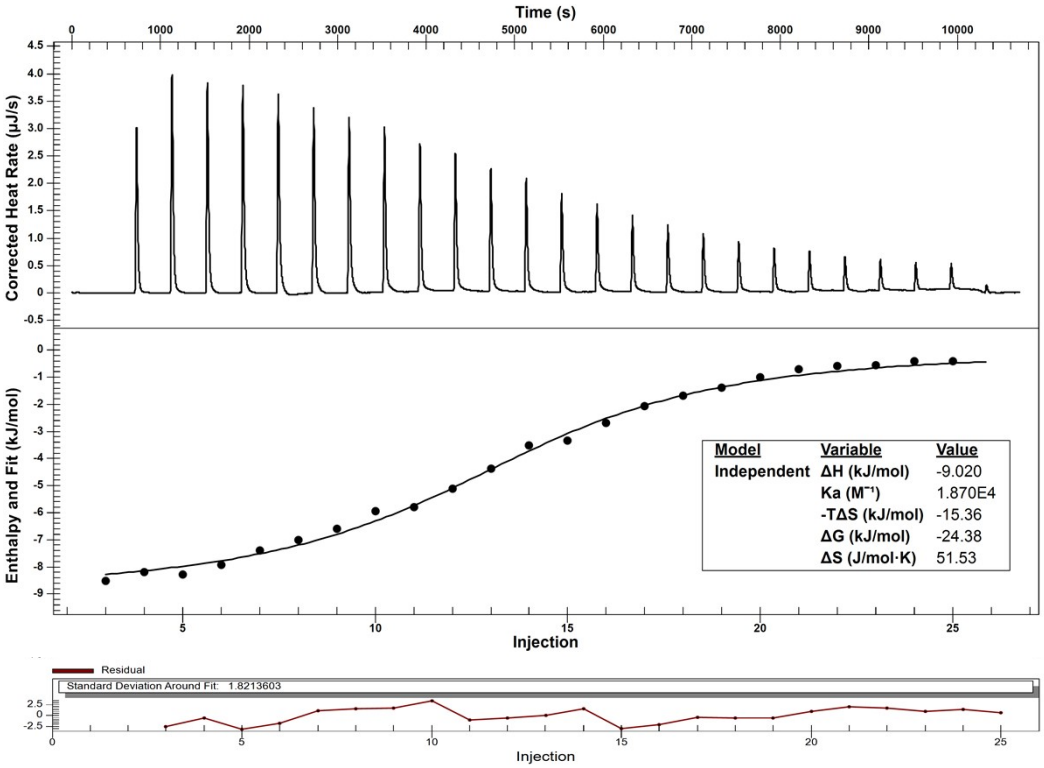
Time (s)
Corrected Heat Rate (µJ/s)
Enthalpy and Fit (kJ/mol)
Injection
Model Variable Value
Independent ΔH (kJ/mol) -9.020
Ka (M⁻¹) 1.870E4
-TΔS (kJ/mol) -15.36
ΔG (kJ/mol) -24.38
ΔS (J/mol·K) 51.53
Residual
Standard Deviation Around Fit: 1.8213603
Injection

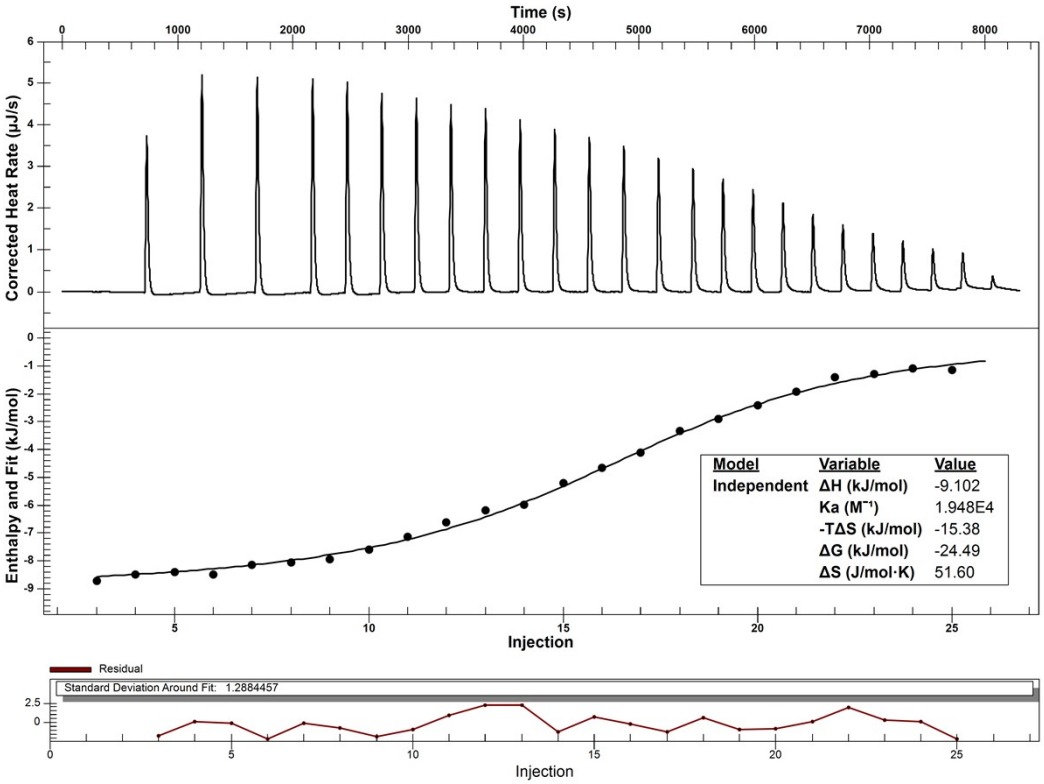
Time (s)
Corrected Heat Rate (µJ/s)
Enthalpy and Fit (kJ/mol)
Injection
Model Variable Value
Independent ΔH (kJ/mol) -9.102
Ka (M⁻¹) 1.948E4
-TΔS (kJ/mol) -15.38
ΔG (kJ/mol) -24.49
ΔS (J/mol·K) 51.60
Residual
Standard Deviation Around Fit: 1.2884457
Injection

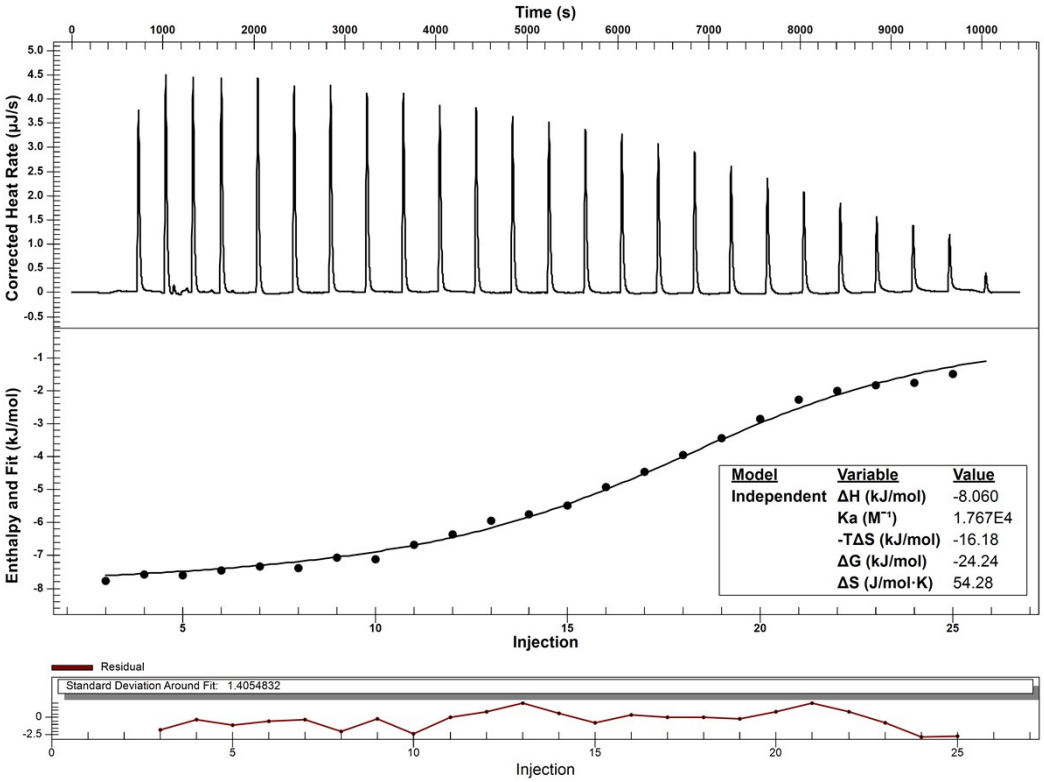

Fig. S15 Results from three independent ITC titrations of cavitand **H** (0.5 mmol/L) with P6 (5 mmol/L) in 5% (v/v) MeOH/water. The raw titration curves (top), the corresponding reaction heat obtained from the integration of each injection peak (middle), and residual plot of the fit (bottom).

Table S6. Triplicate ITC data for the P6@**H** complex

	1	2	3	Mean ± SD (K_a / M^{-1})	RSD / %
K (M^{-1})	1.87×10^4	1.95×10^4	1.77×10^4	$(1.86 \pm 0.09) \times 10^4$	4.84
ΔH (kJ/mol)	−9.02	−9.10	−8.06	−8.73 ± 0.58	6.60
ΔG (kJ/mol)	−24.38	−24.49	−24.24	−24.37 ± 0.13	0.51
ΔS (J/mol·K)	51.53	51.60	54.28	52.47 ± 1.57	3.00
Residual SD	1.82	1.29	1.41	-	-

Note: values are rounded to two decimal places

The binding behaviors of P5-P8 in cavitand **H'** was first investigated (Fig. S16). The results showed that the pyridine guests exhibited broad complex peaks in the upfield region, indicating a relatively fast on-off exchange rate of the guests within the cavity.[7-11] As the alkyl chain length increased, the δ values of the terminal CH_3 group did not change significantly. Meanwhile, broad peaks appeared in the δ = 0-2 ppm range, corresponding to the alkyl chains of the guests that did not enter the cavity. This indicates that the complexation mode of 4-alkylpyridines with cavitand **H'** is similar to the behavior of **H'** with linear alcohols: driven by the hydrophobic effect, the alkyl tail

of the guest inserts into the cavity.[2] Concurrently, the number of alkyl segments embedded within the cavity and the position of the terminal CH_3 group do not change with increasing chain length, while the unembedded portion coils around the cavity opening.

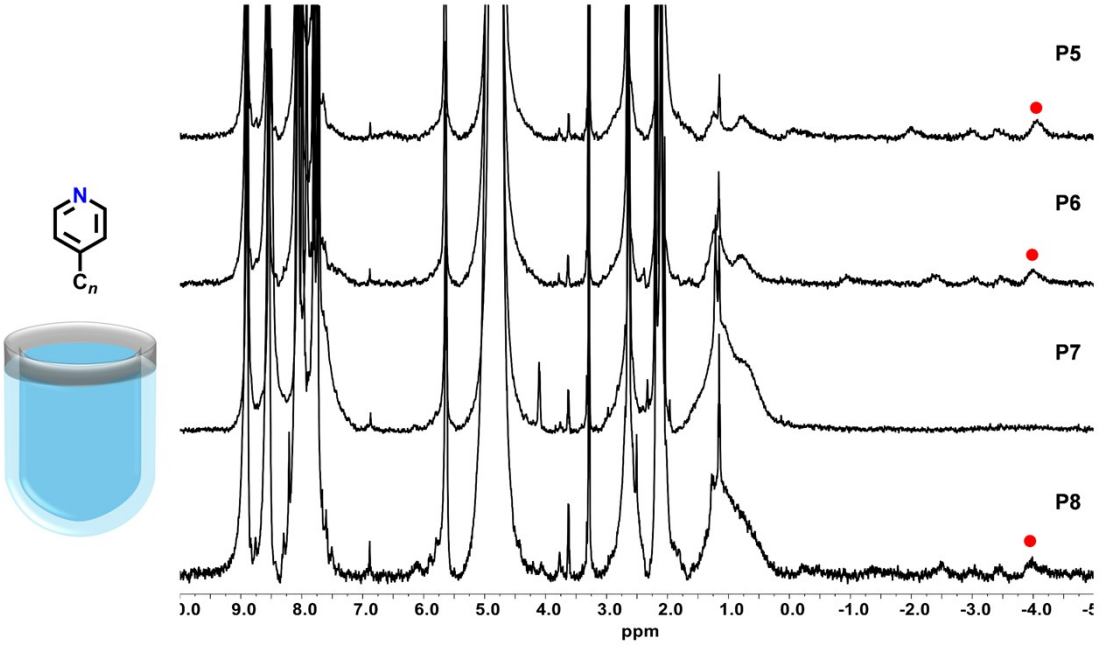

Fig. S16 ^{1}H NMR (600 MHz, D_2O, 298 K) spectra of **H'** bound to 4-alkylpyridine guests. The red dots correspond to the terminal CH_3 groups of guests.

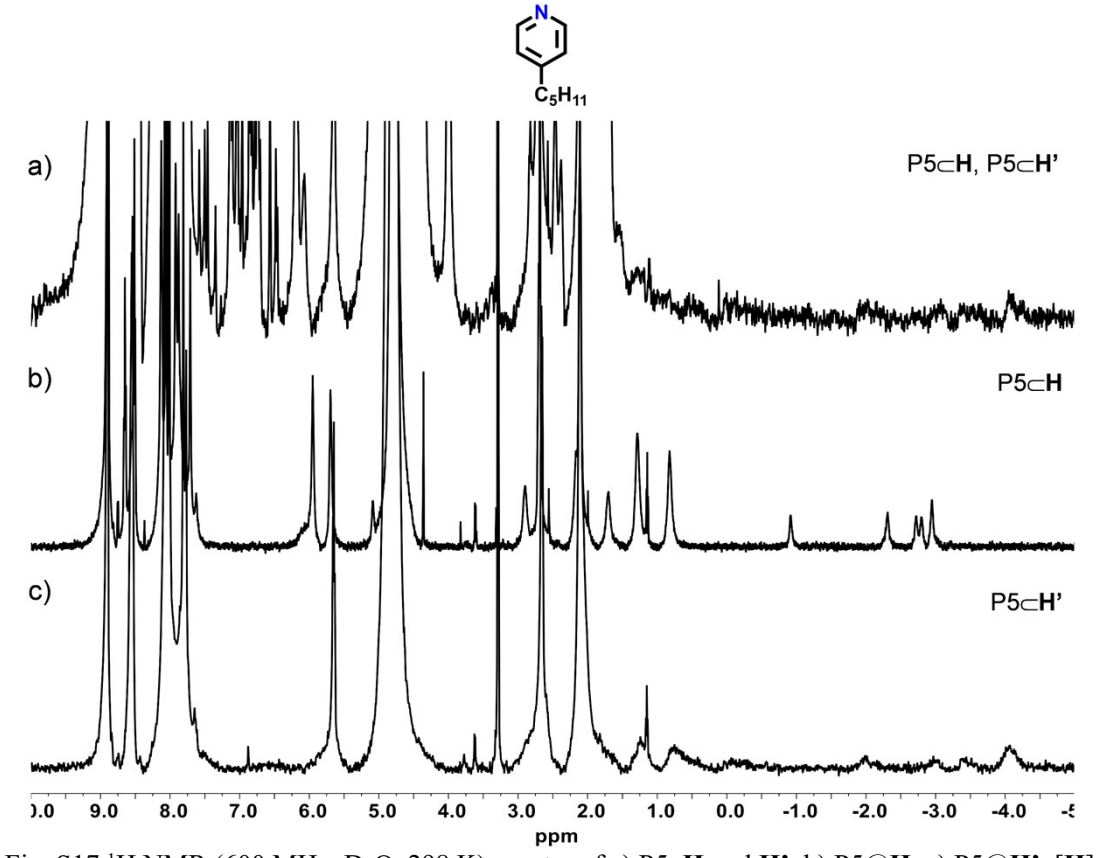

Fig. S17 ^{1}H NMR (600 MHz, D_2O, 298 K) spectra of a) P5, **H** and **H'**, b) P5@**H**, c) P5@**H'**. [**H**] = [**H'**] = 1 mmol/L, [P5] = 0.2 mmol/L.

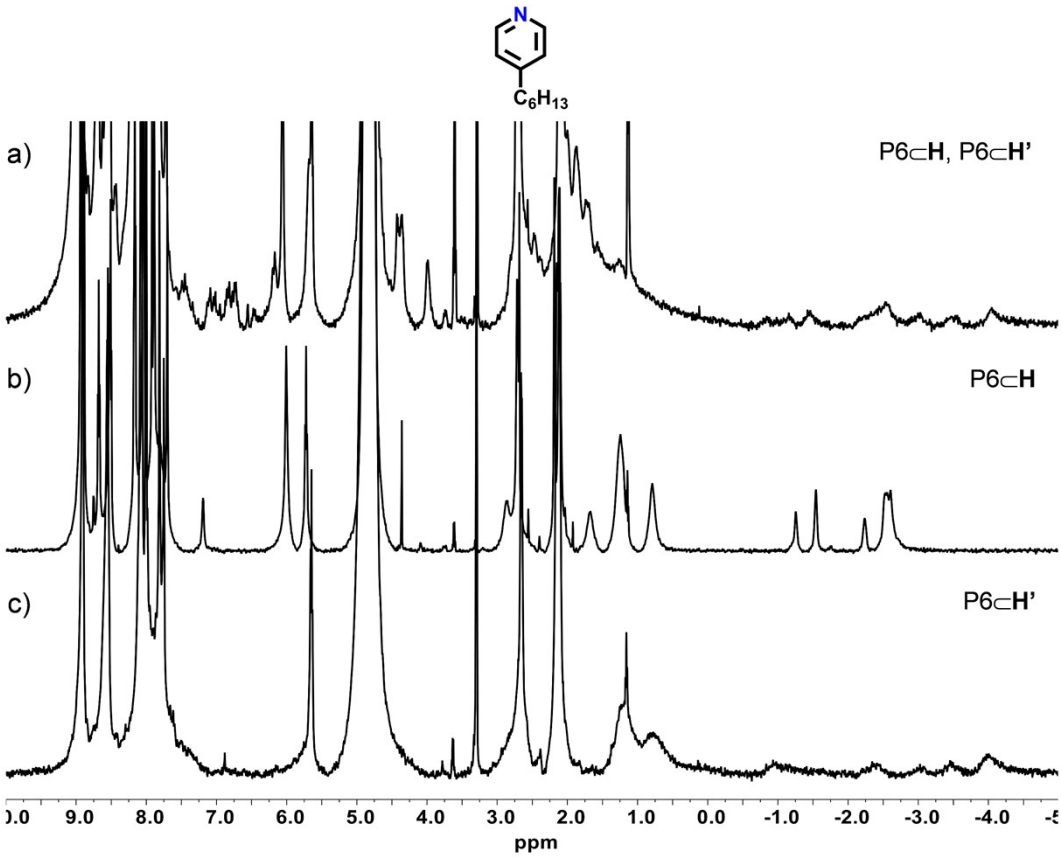

Fig. S18 ^{1}H NMR (600 MHz, D_2O, 298 K) spectra of a) P6, **H** and **H'**, b) P6@**H**, c) P6@**H'**. [**H**] = [**H'**] = 1 mmol/L, [P6] = 0.2 mmol/L.

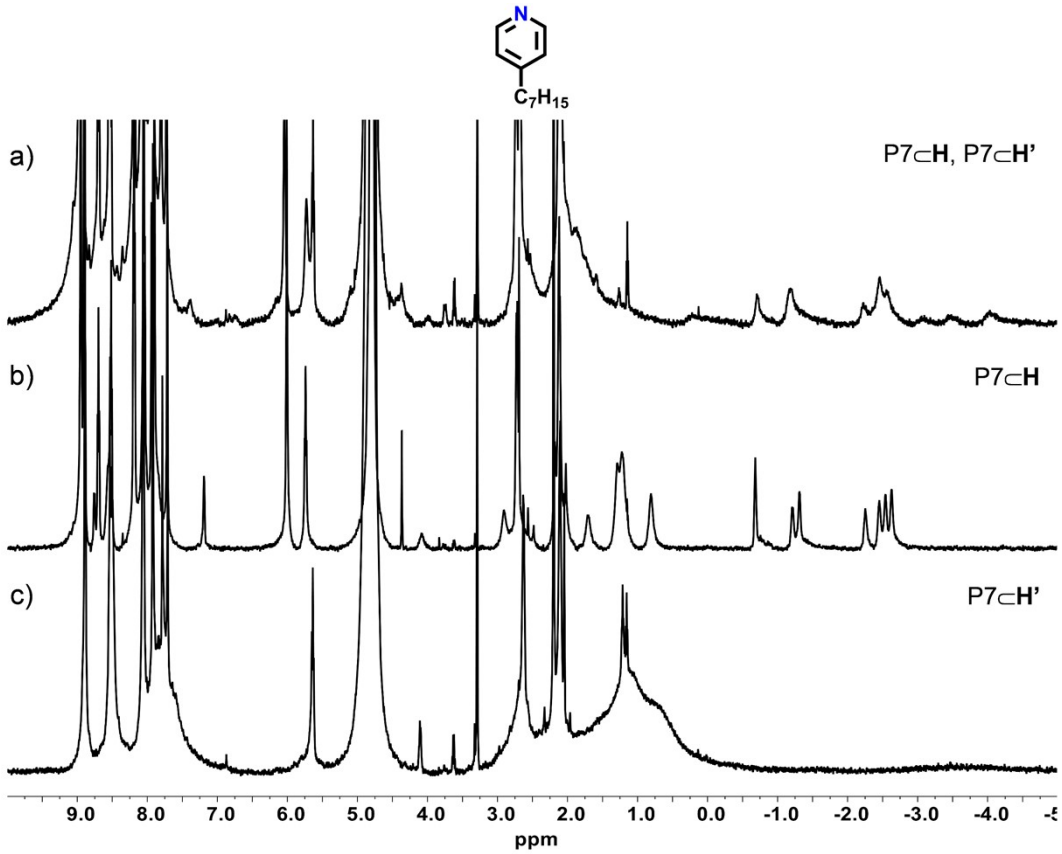

Fig. S19 ^{1}H NMR (600 MHz, D_2O, 298 K) spectra of a) P7, **H** and **H'**, b) P7@**H**, c) P7@**H'**. [**H**] = [**H'**] = 1 mmol/L, [P7] = 0.2 mmol/L.

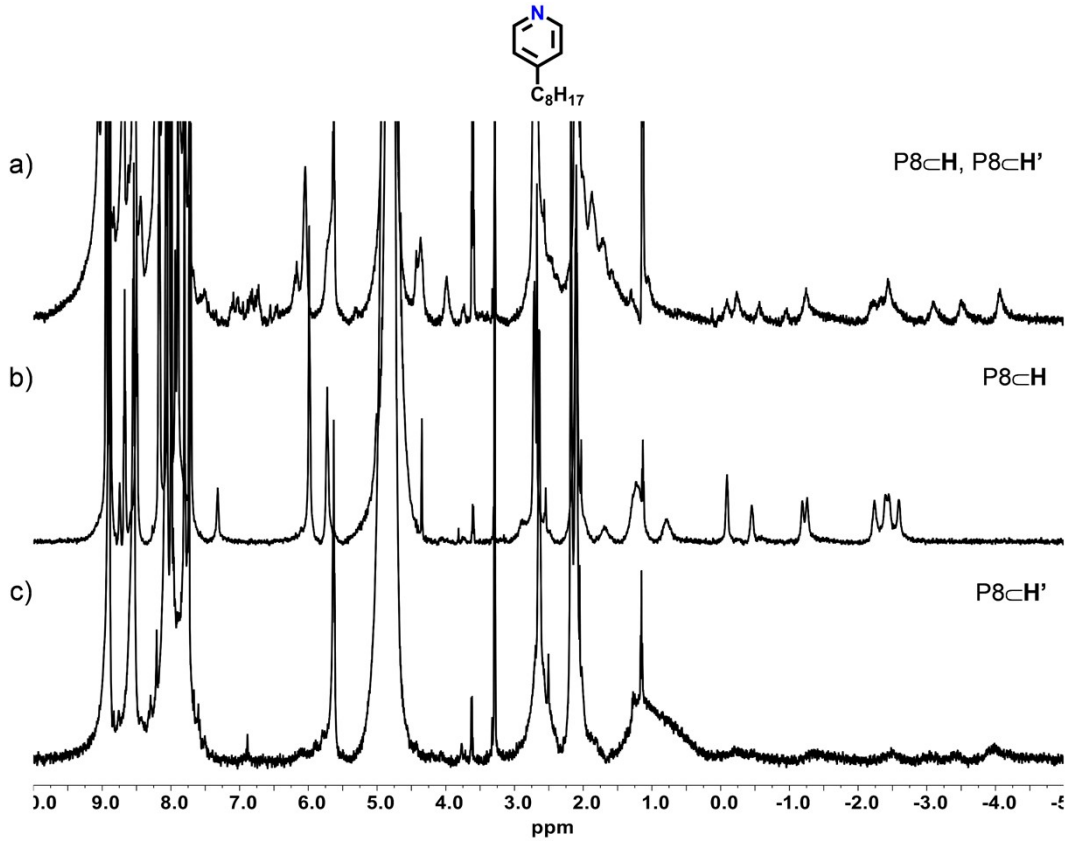

Fig. S20 ^{1}H NMR (600 MHz, D_2O, 298 K) spectra of a) P8, **H** and **H'**, b) P8@**H**, c) P8@**H'**. [**H**] = [**H'**] = 1 mmol/L, [P8] = 0.2 mmol/L.

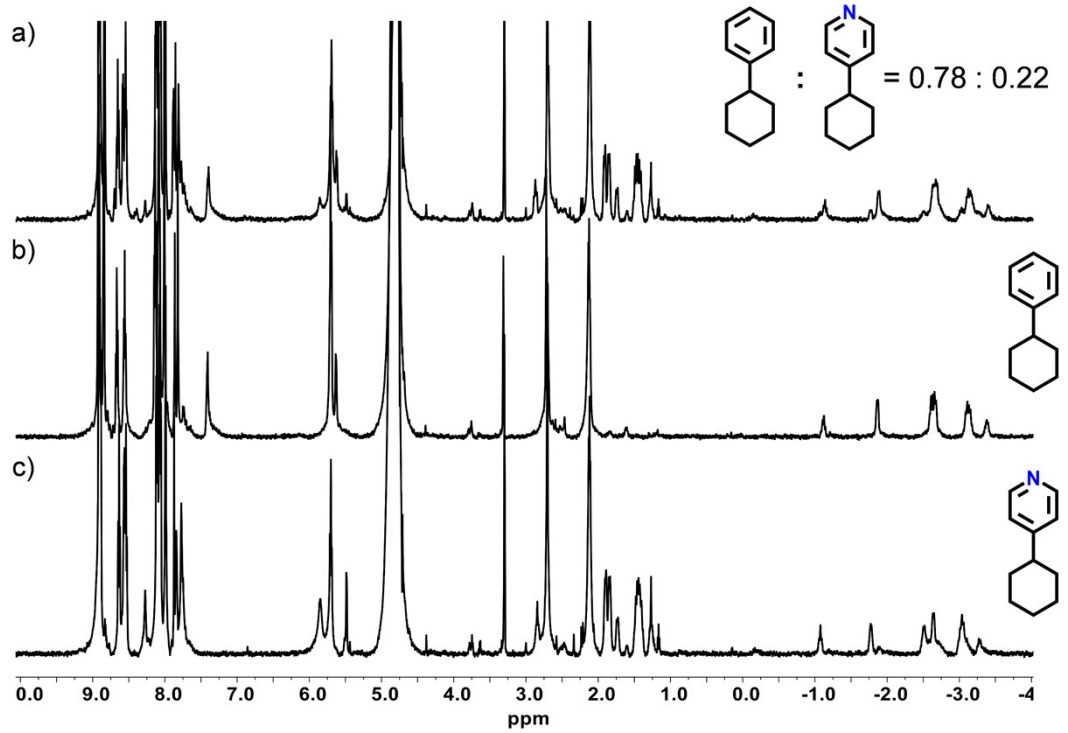

Fig. S21 ^{1}H NMR (600 MHz, D_2O, 298 K) spectra of a) cyclohexylbenzene, 4-cyclohexylpyridine and **H**, b) cyclohexylbenzene@**H**, c) 4-cyclohexylpyridine@**H**. [**H**] = [cyclohexylbenzene] = [4-cyclohexylpyridine] = 1 mmol/L.

The characteristic peaks of cyclohexylbenzene@**H** (pink dots, δ −3.40 ppm) and

4-cyclohexylpyridine@**H** (orange dots, δ −0.77 ~ −0.80 ppm across replicates, see individual spectra for exact values) are non-overlapping (Fig. S22). For individual complexes, the selected peak of cyclohexylbenzene@**H** (1 proton) was normalized to 1.00, and the selected peak of 4-cyclohexylpyridine@**H** (2 protons) was normalized to 2.00. In the competition spectra, the integral of the cyclohexylbenzene@**H** peak was set as the reference and normalized to 1.00. The observed integrals of the 4-cyclohexylpyridine@**H** peak were 0.56, 0.51, and 0.56 for the three replicates. Dividing these values by 2.00 gives the relative molar amounts of bound 4-cyclohexylpyridine: 0.28, 0.26, and 0.28. Thus, the molar ratios (cyclohexylbenzene@**H**:4-cyclohexylpyridine@**H**) are 1:0.28, 1:0.26, and 1:0.28, which correspond to 0.78:0.22, 0.80:0.20, and 0.78:0.22, respectively. Triplicate measurements yielded an RSD of 1.5%, indicating good reproducibility.

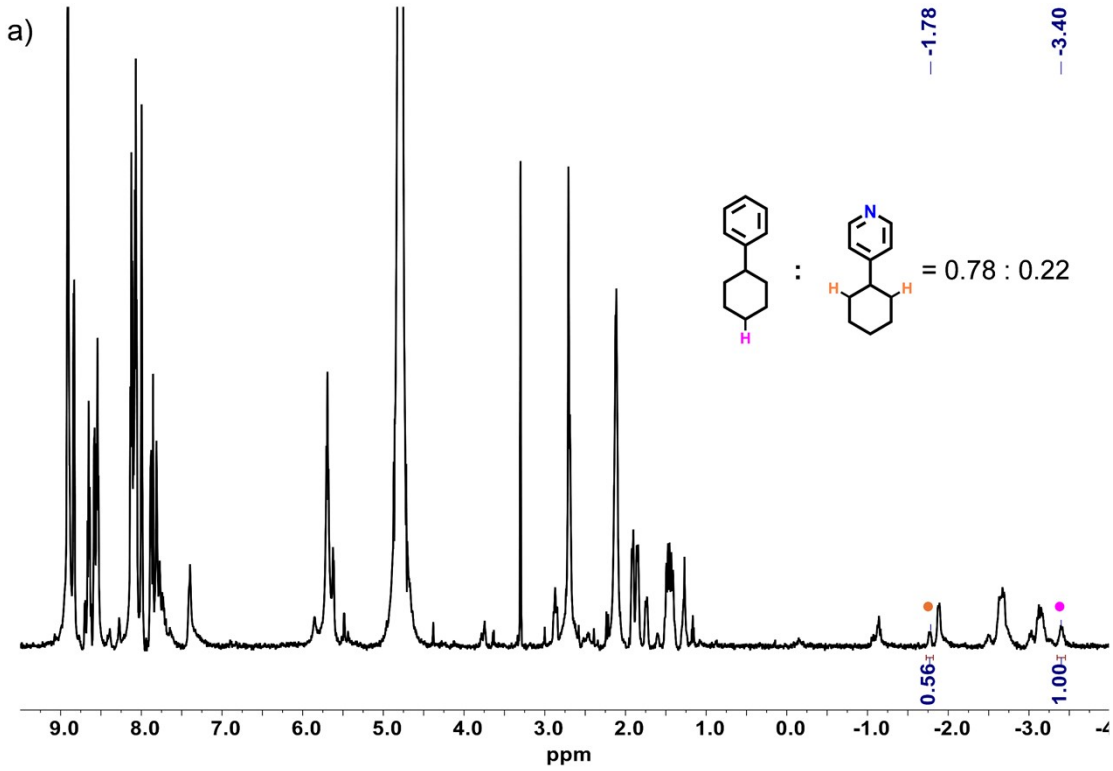

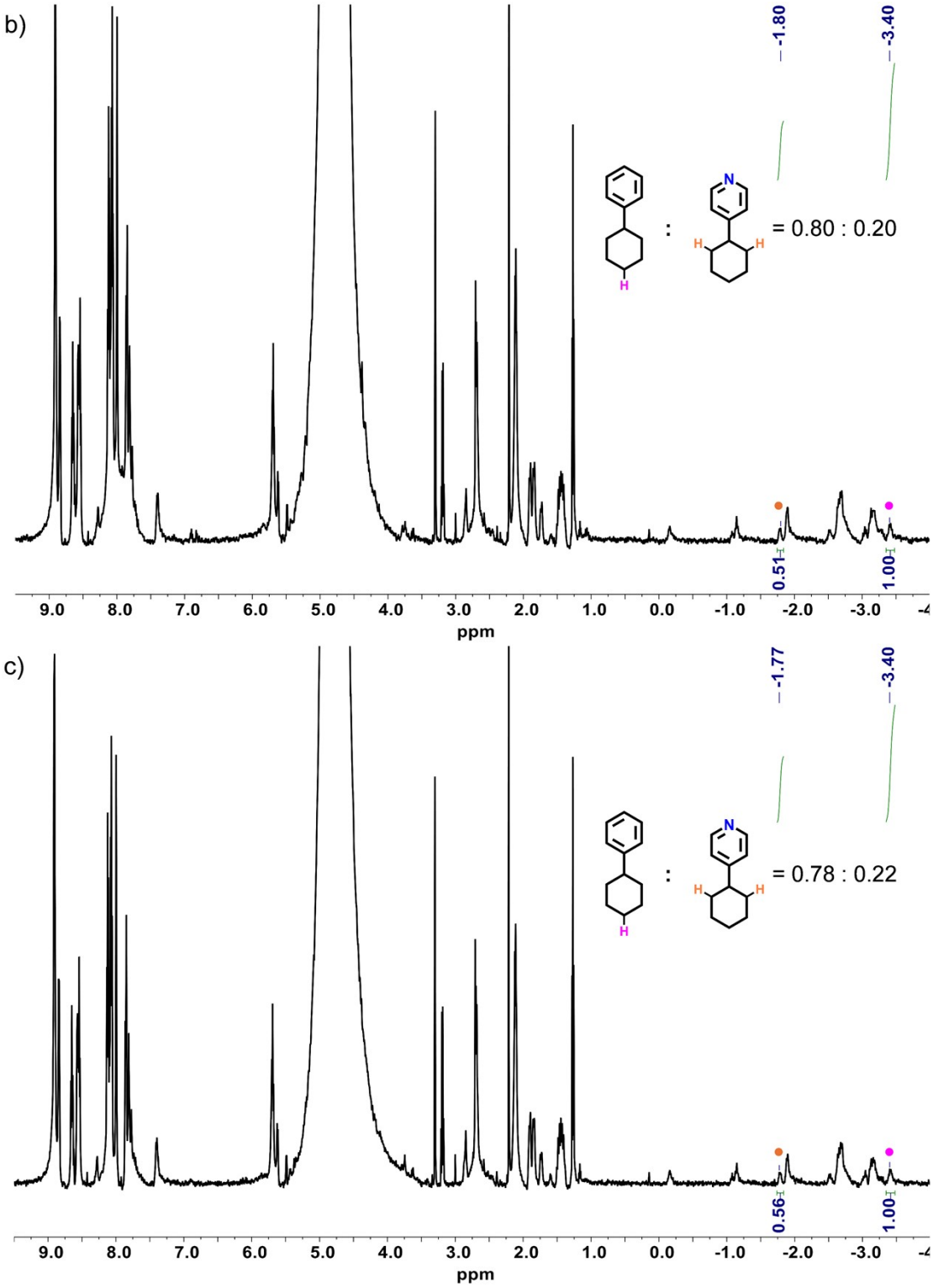

Fig. S22 ^{1}H NMR (600 MHz, D_2O, 298 K) spectra of three independent replicate competition experiments (a, b, c) of cyclohexylbenzene, 4-cyclohexylpyridine and **H**. The pink dots indicate the characteristic peak of cyclohexylbenzene@**H**, and orange dots indicate 4-cyclohexylpyridine@**H**. [**H**] = [cyclohexylbenzene] = [4-cyclohexylpyridine] = 1 mmol/L.

Based on the K_a value obtained from three independent experiments (Table S7), the c value was calculated to be 35.4. This value falls within the conventionally recommended range of 5-500, indicating favorable experimental conditions for reliable

ITC fitting. The titration curve exhibits a clear sigmoidal shape with a distinct inflection point and a terminal plateau, the fit residuals are randomly distributed (within –1 to 2), and the RSD of K_a is 0.83%. Thus, the results are reliable.

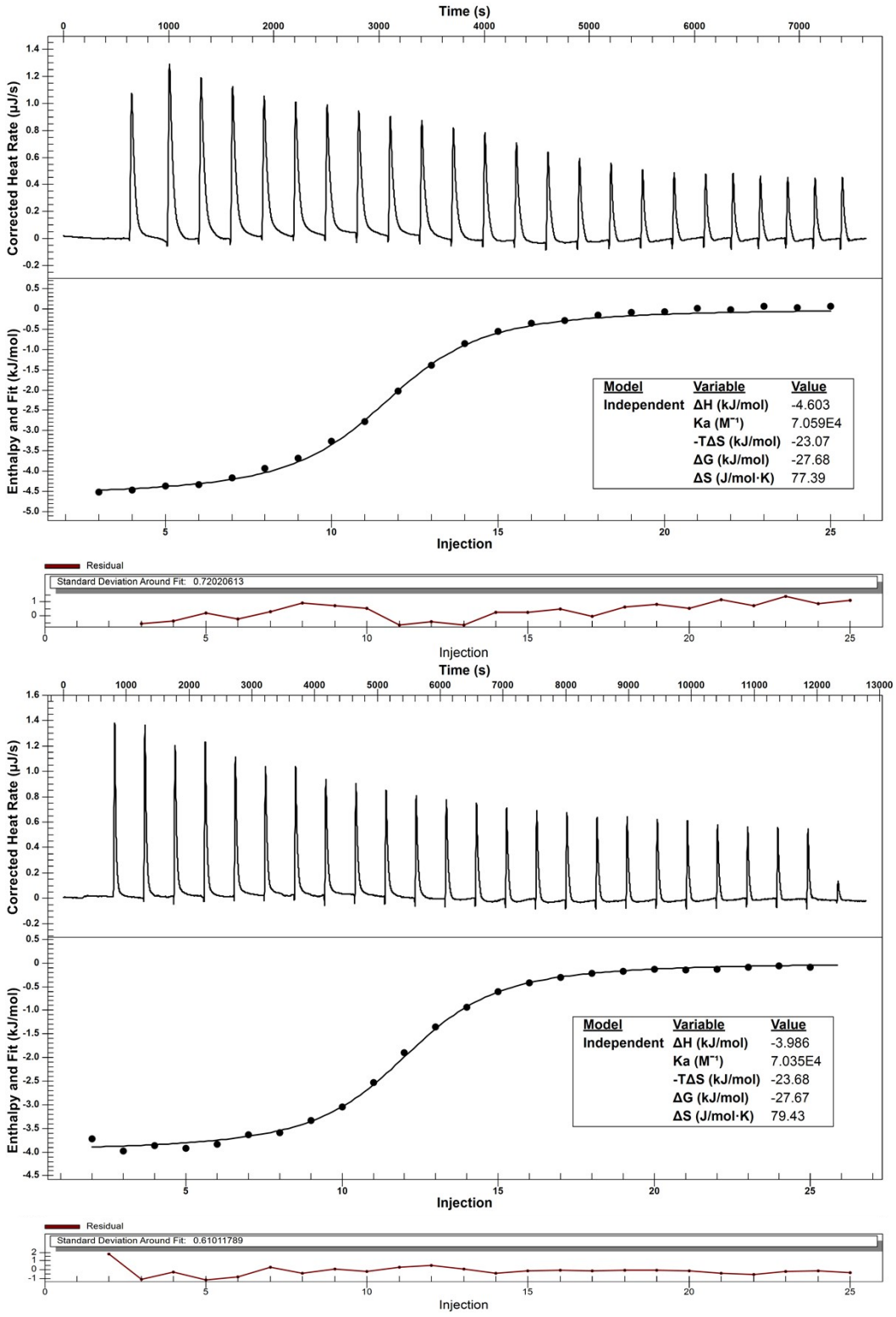

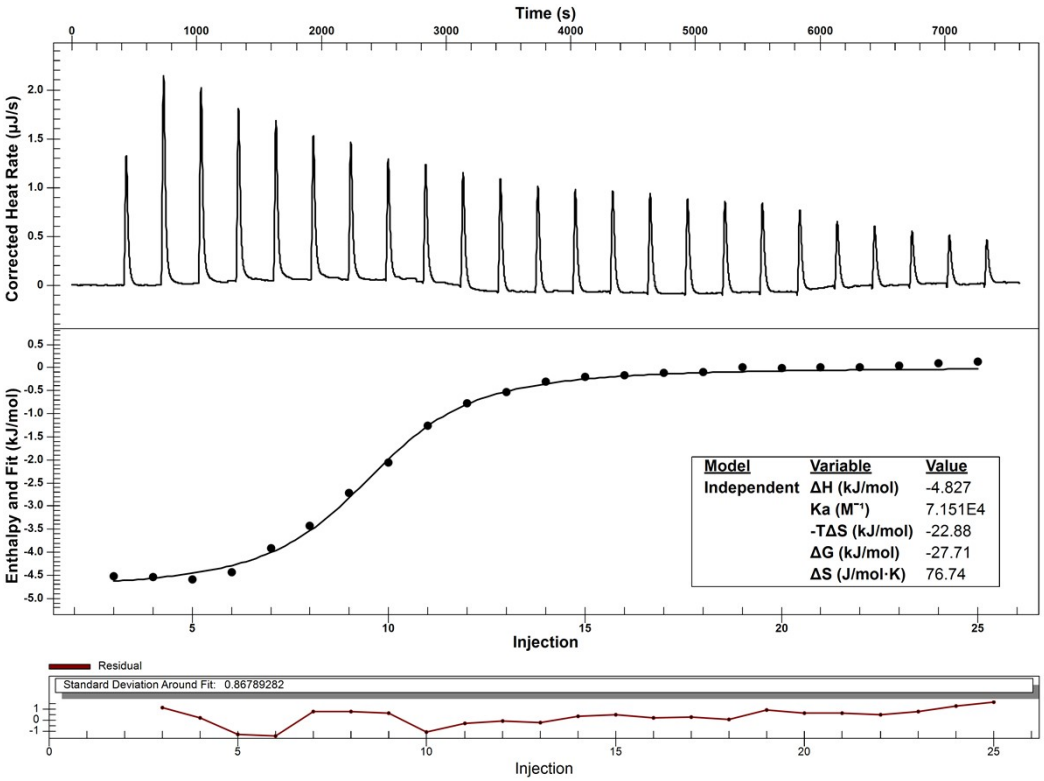

Fig. S23 Results from three independent ITC titrations of cavitand **H** (0.5 mmol/L) with cyclohexylbenzene (5 mmol/L) in 5% (v/v) MeOH/water. The raw titration curves (top), the corresponding reaction heat obtained from the integration of each injection peak (middle), and residual plot of the fit (bottom).

Table S7. Triplicate ITC data for the cyclohexylbenzene@**H** complex

	1	2	3	Mean ± SD (K_a / M^{-1})	RSD / %
K (M^{-1})	7.06×10^4	7.04×10^4	7.15×10^4	$(7.08 \pm 0.06) \times 10^4$	0.83
ΔH (kJ/mol)	−4.60	−3.99	−4.83	−4.47 ± 0.43	9.70
ΔG (kJ/mol)	−27.68	−27.67	−27.71	−27.69 ± 0.02	0.08
ΔS (J/mol·K)	77.39	79.43	76.74	77.85 ± 1.40	1.80
Residual SD	0.72	0.61	0.87	-	-

Note: values are rounded to two decimal places

For 4-cyclohexylpyridine@**H** complex, based on the K_a value obtained from three independent experiments (Table S8), the c value was calculated to be 18.3. This value falls within the conventionally recommended range of 5-500, indicating favorable experimental conditions for reliable ITC fitting. The titration curve exhibits a clear sigmoidal shape with a distinct inflection point and a terminal plateau, the fit residuals are randomly distributed (within –5 to 5), and the RSD of K_a is 2.99%. Thus, the results

are reliable.

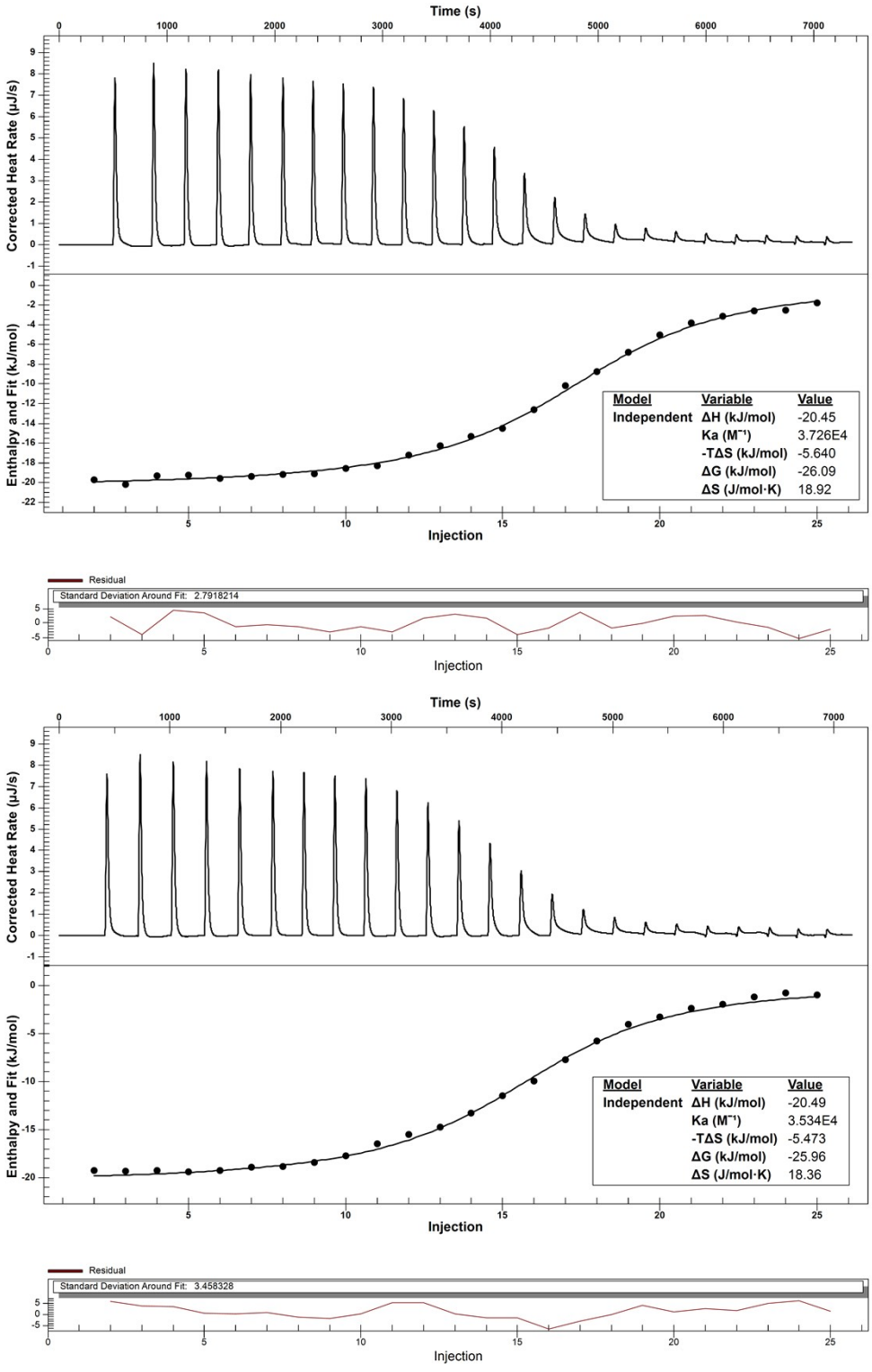

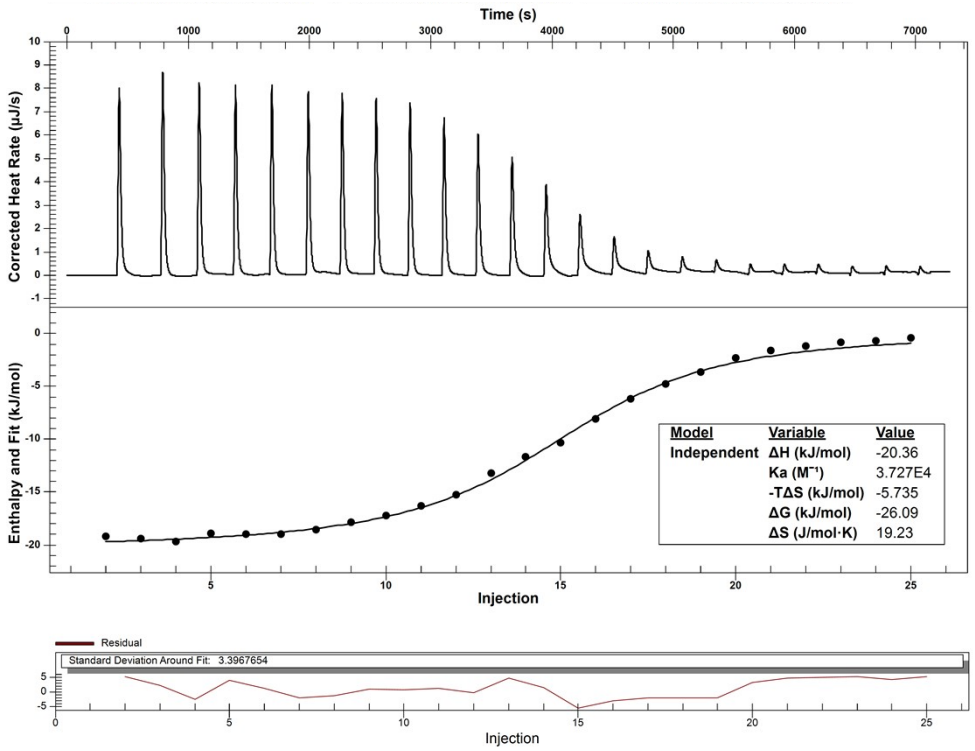

Fig. S24 Results from three independent ITC titrations of cavitand **H** (0.5 mmol/L) with 4-cyclohexylpyridine (5 mmol/L) in 5% (v/v) MeOH/water. The raw titration curves (top), the corresponding reaction heat obtained from the integration of each injection peak (middle), and residual plot of the fit (bottom).

Table S8. Triplicate ITC data for the 4-cyclohexylpyridine@**H** complex

	1	2	3	Mean ± SD (K_a / M^{-1})	RSD / %
K (M^{-1})	3.73×10^4	3.53×10^4	3.73×10^4	$(3.66 \pm 0.12) \times 10^4$	3.14
ΔH (kJ/mol)	−20.45	−20.49	−20.36	−20.43 ± 0.07	0.34
ΔG (kJ/mol)	−26.09	−25.96	−26.09	−26.05 ± 0.08	0.31
ΔS (J/mol·K)	18.92	18.36	19.23	18.84 ± 0.44	2.34
Residual SD	2.79	3.46	3.40	-	-

Note: values are rounded to two decimal places

4. Recognition behaviors of 4-alkylaniline and 4-alkylnitrobenzene by cavitand H

The sharp and well-resolved complexation peaks of 4-alkylanilines in the upfield region indicates the formation of stable complexes (Fig. S25). The behavior within the cavity shows that for NB5, the terminal CH_3 group exhibits the smallest Δδ value (Table S9), indicating it resides deepest within the cavity in an "extended" conformation. For NB6, the terminal CH_3 group still shows the smallest Δδ value, but its |Δδ| value is smaller than that of NB5, suggesting that while the terminal CH_3 group remains deepest, the conformation has changed to "coiled". For NB7-NB8, the CH_2 group rather than the terminal CH_3 resides deepest, confirming that the alkyl tail adopts a "folded" conformation. Examination of the aromatic region reveals that the NB_α protons on the aniline group of NB5 and NB6 undergo downfield shifts, while those of NB7-NB8 experience upfield shifts, indicating shielding. In contrast, all NB_β protons are shielded with Δδ values ranging from −0.42 ppm to 0 ppm. This may be attributed to the partial positive charge on $-NH_2$, which could lead to repulsion with the upper rim of cavitand **H**, causing the aniline group move to the cavity opening. Meanwhile, the 4-alkylanilines also affect the H_a and H_d protons on the upper rim of cavitand **H** (Fig. S29a and Table S11), with values close to those observed for alkylbenzenes, suggesting the possible presence of cation-π interactions between the guest and the host.

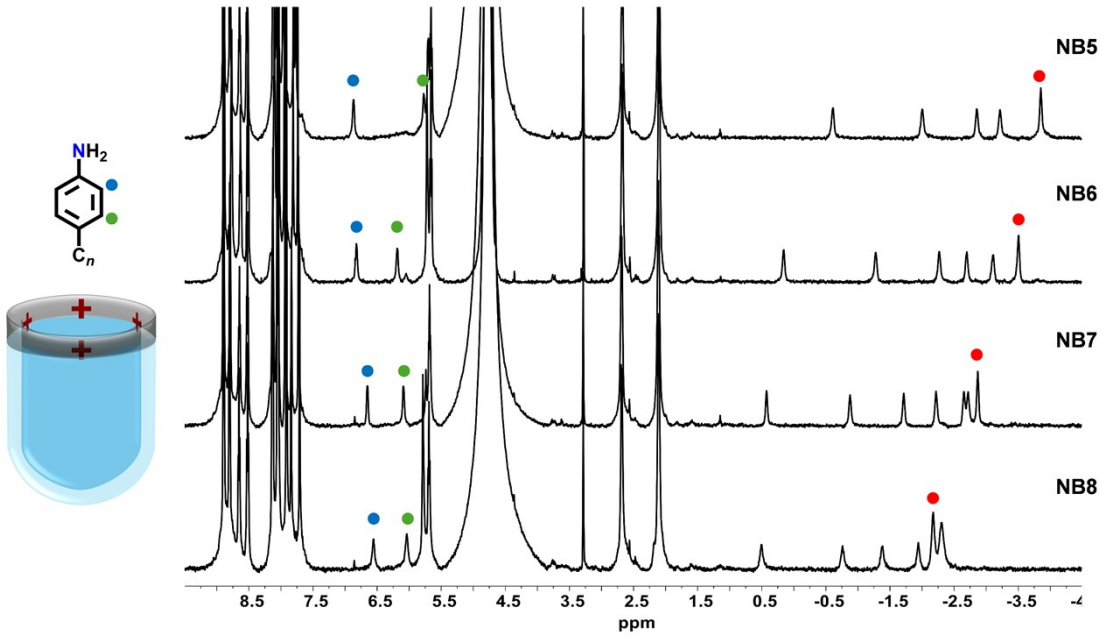

Fig. S25 ^{1}H NMR (600 MHz, D_2O, 298 K) spectra of **H** bound to 4-alkylaniline guests. The blue and green dots represent the positions of the α-CH protons (NB_α) and β-CH protons (NB_β) on the aniline group, respectively, and the red dots correspond to the terminal CH_3 groups of guests.

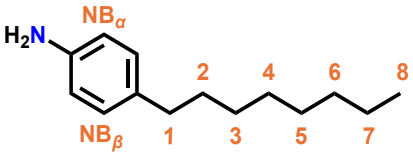

Fig. S26 The structure of NB8.

Table S9. Δδ values of alkyl chains for 4-alkylaniline guests upon bound to **H**

G@**H** / Δδ/ppm / C_n	NB5 @**H**	NB6 @**H**	NB7 @**H**	NB8 @**H**
NB$_\alpha$	0.21	0.16	−0.01	−0.11
NB$_\beta$	−0.42	0	−0.11	−0.15
1	−2.90	−2.13	−1.87	−1.79
2	−3.39	−2.66	−2.26	−2.14
3	−4.00	−3.42	−2.86	−2.53
4	−4.37	−3.85	−3.37	−3.09
5	−4.64	−4.26	−3.80	−3.33
6		−4.30	−3.87	−3.46
7			−3.66	−3.46
8				−2.97

The upfield complexation peaks of 4-alkylnitrobenzenes (NO5-NO8) appeared sharp and well-resolved (Fig. S27), indicating the formation of relatively stable host–guest complexes. For all chain lengths, the moiety residing deepest within the cavity was a CH_2 group rather than the terminal CH_3 (Table S10), indicating that the alkyl chains of the guests were "folded" conformations inside the cavity. Compared to other alkyl groups, the $|\Delta\delta|$ values of the terminal CH_3 groups for NO6-NO8 exceeded that of the α-CH_2 group adjacent to the nitrobenzene moiety and became the smallest, suggesting a higher degree of folding and positioning the terminal CH_3 group closest to the cavity opening. Meanwhile, both NO_α and NO_β protons on the nitrobenzene ring experienced significant shielding, with $\Delta\delta$ values reaching approximately −1.20 ppm and −2.50 ppm, indicating deep penetration of the nitrobenzene group into the cavity of the cationic cavitand **H**. Similarly, the 4-alkylnitrobenzenes also affect the H_a and H_d protons on the upper rim of cavitand **H** (Fig. S29b and Table S12). The behavior is similar to that observed for 4-alkylpyridines.

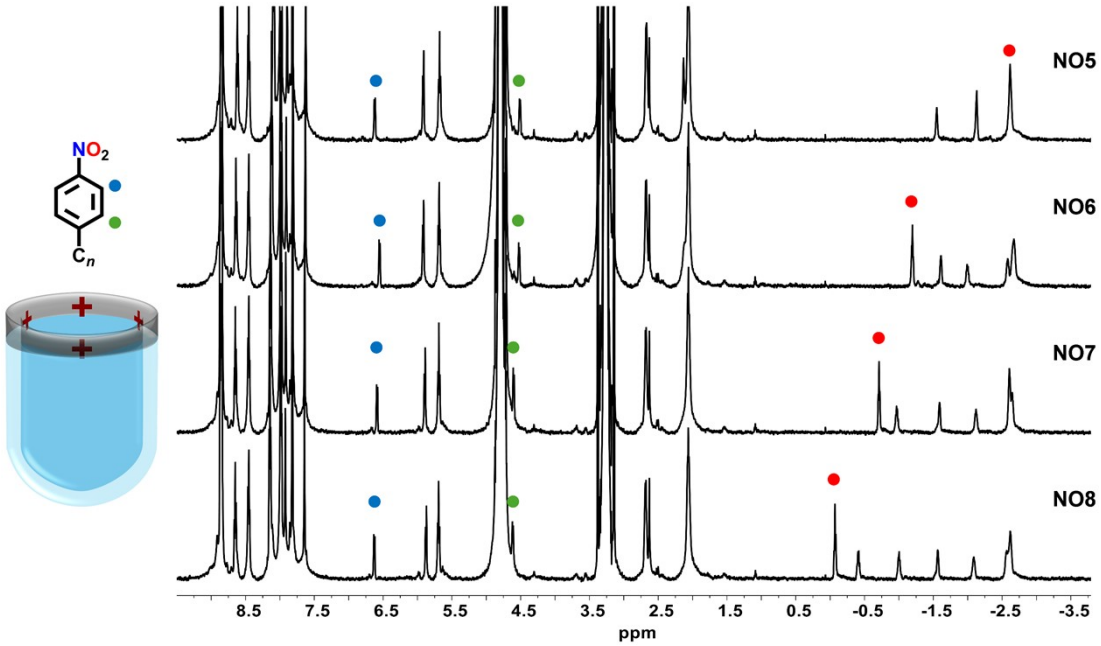

Fig. S27 ^{1}H NMR (600 MHz, D_2O, 298 K) spectra of **H** bound to 4-alkylnitrobenzene guests. The blue and green dots represent the positions of the α-CH protons (NO_α) and β-CH protons (NO_β) on the nitrophenyl, respectively, and the red dots correspond to the terminal CH_3 groups of guests.

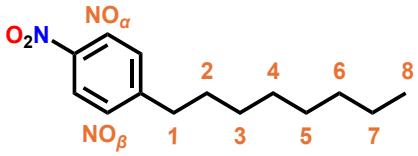

Fig. S28 The structure of NO8.

Table S10. Δδ values of alkyl chains for 4-alkylnitrobenzene guests upon bound to **H**

G@**H** / Δδ/ppm / C_n	NO5 @**H**	NO6 @**H**	NO7 @**H**	NO8 @**H**
NO_α	−1.17	−1.24	−1.21	−1.17
NO_β	−2.56	−2.55	−2.45	−2.44
1	−3.97	−4.03	−4.01	−3.99
2	−3.49	−3.35	−3.48	−3.45
3	−3.65	−3.61	−3.64	−3.59
4	−3.65	−3.70	−3.68	−3.65
5	−3.25	−3.70	−3.64	−3.65
6		−1.83	−2.00	−2.03
7			−1.34	−1.43
8				−0.70

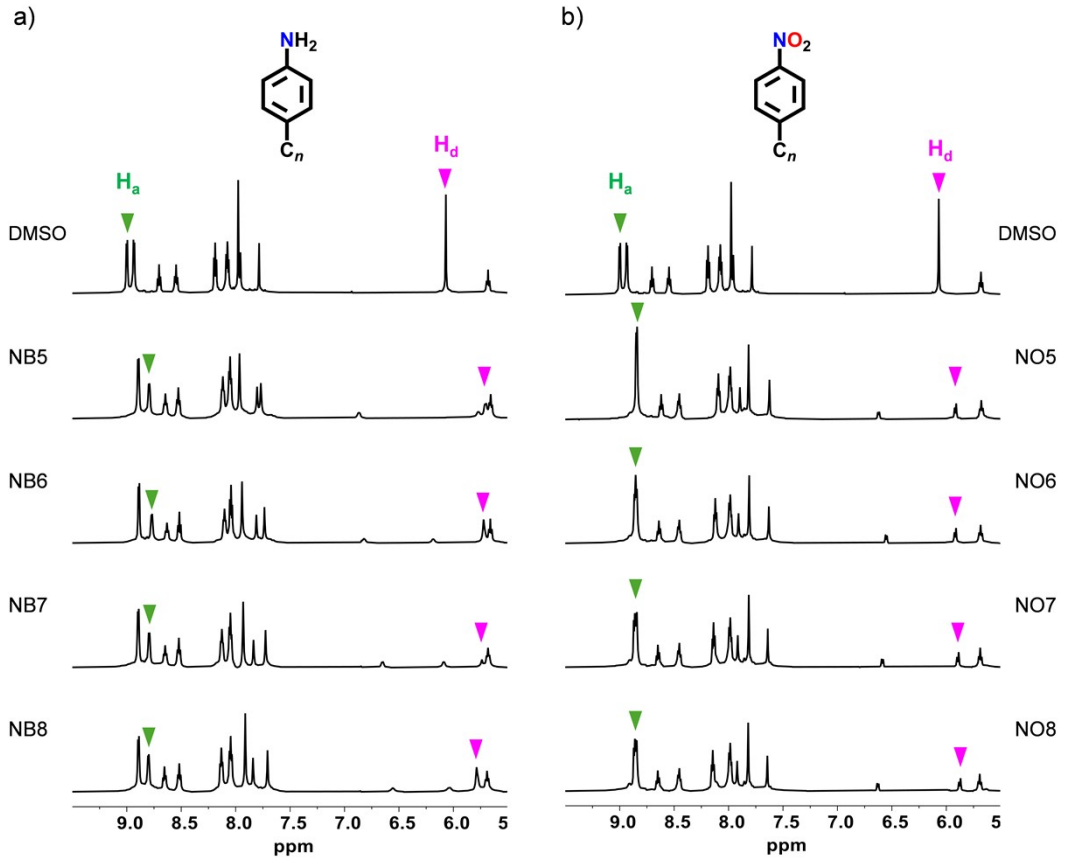

Fig. S29 Partial ^{1}H NMR (600 MHz, D_2O, 298 K) spectra (5.5 to 9.5 ppm) of **H** bound to a) 4-alkylaniline and b) 4-alkylnitrobenzene guests. The green and pink triangles indicate the H_a and H_d positions of **H** after bound to guests.

Table S11. The Δδ values for H_a and H_d of **H** bound to 4-alkylaniline guests

H@G / Δδ/ppm / C_n	**H**@NB5	**H**@NB6	**H**@NB7	**H**@NB8
H_a	−0.20	−0.22	−0.20	−0.19
H_d	−0.36	−0.35	−0.33	−0.28

Table S12. The Δδ values for H_a and H_d of **H** bound to 4-alkylnitrobenzene guests

H@G / Δδ/ppm / C_n	**H**@NO5	**H**@NO6	**H**@NO7	**H**@NO8
H_a	−0.16	−0.16	−0.16	−0.16
H_d	−0.16	−0.16	−0.18	−0.20

5. Competition experiments for 4-alkylaniline and 4-alkylnitrobenzene

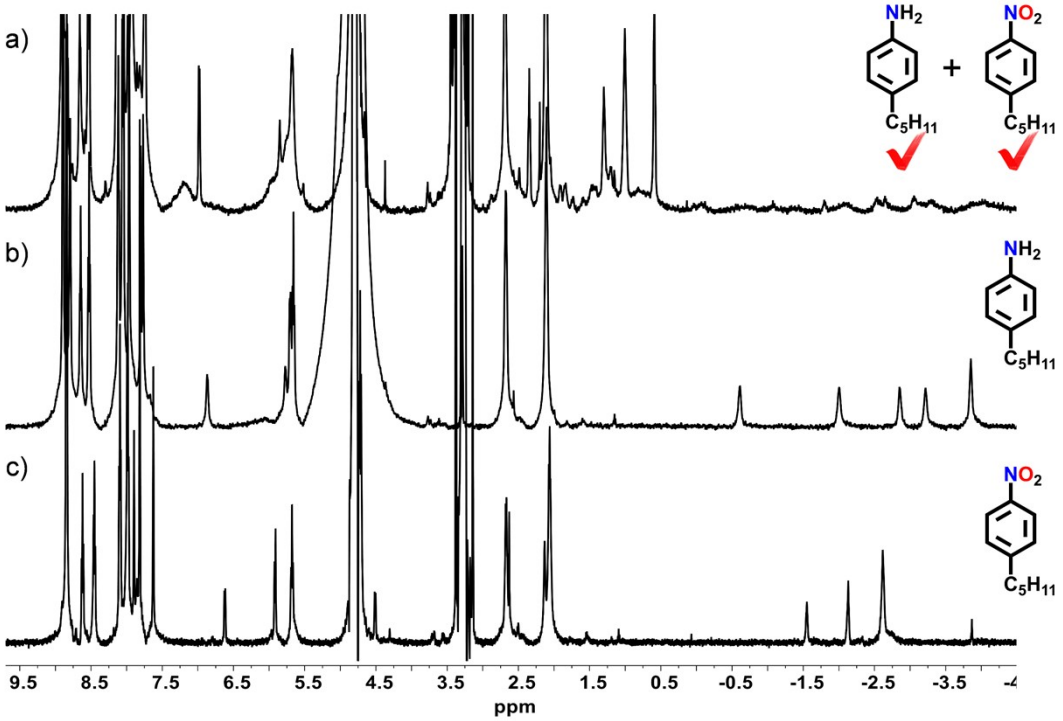

Fig. S30 ^{1}H NMR (600 MHz, D_2O, 298 K) spectra of a) NB5, NO5 and **H**, b) NB5@**H**, c) NO5@**H**. [**H**] = [NB5] = [NO5] = 1 mmol/L. The red checkmarks indicate the guests enter into the cavity of **H**.

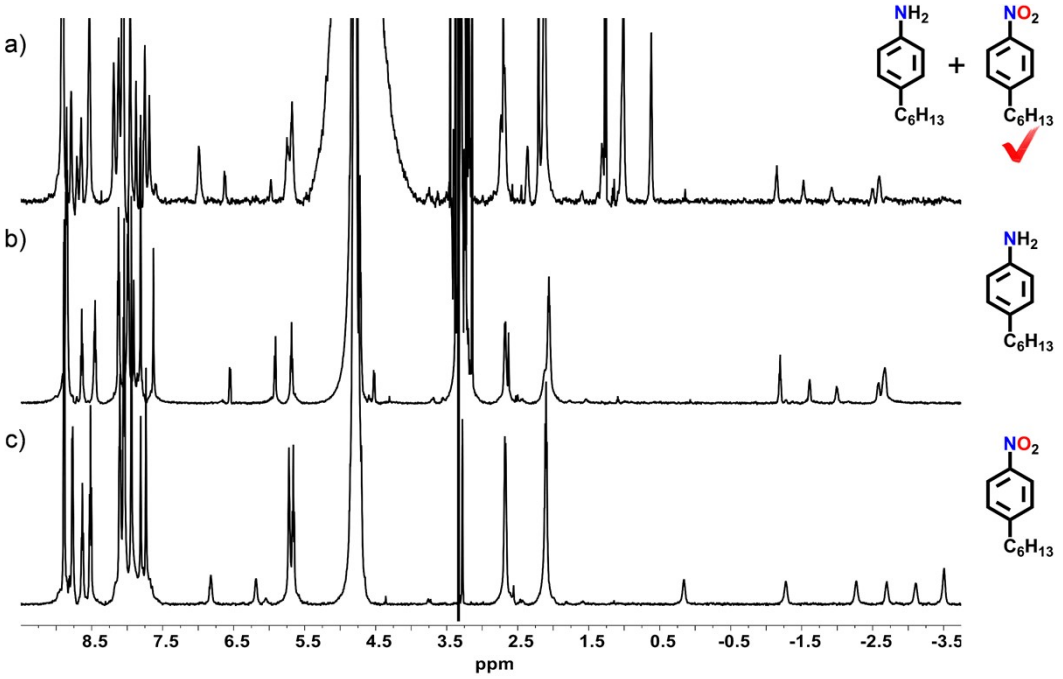

Fig. S31 ^{1}H NMR (600 MHz, D_2O, 298 K) spectra of a) NB6, NO6 and **H**, b) NB6@**H**, c) NO6@**H**. [**H**] = [NB6] = [NO6] = 1 mmol/L. The red checkmark indicates the guest enters into the cavity of **H**.

Two independent competition experiments for NB6 vs. NO6 both show exclusive encapsulation of NO6 (Fig. S32), confirming the reproducibility of the selectivity.

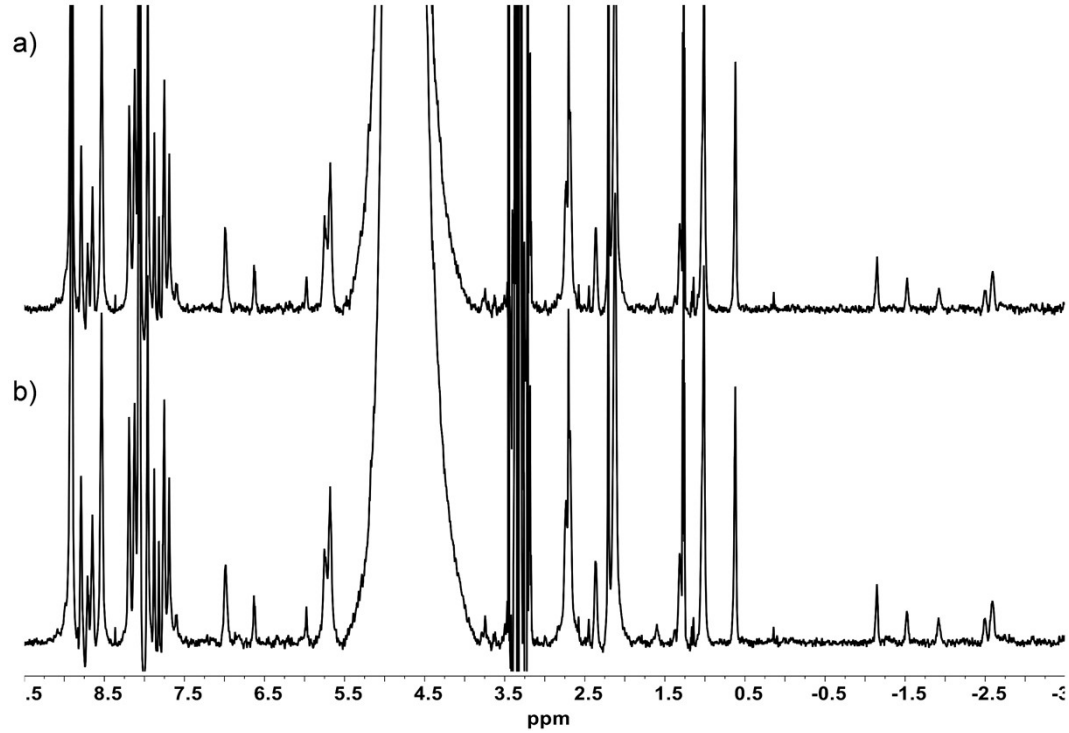

Fig. S32 ^{1}H NMR (600 MHz, D_2O, 298 K) spectra of two independent replicate competition experiments (a and b) of NB6, NO6 and **H**. [**H**] = [NB6] = [NO6] = 1 mmol/L.

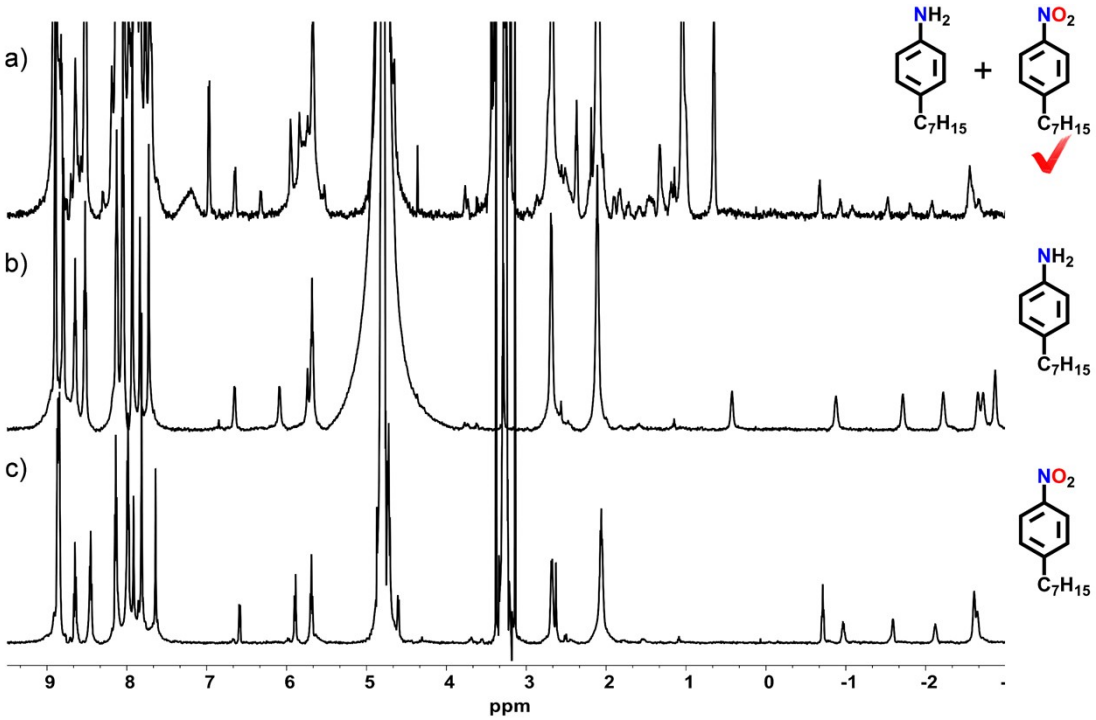

Fig. S33 ^{1}H NMR (600 MHz, D_2O, 298 K) spectra of a) NB7, NO7 and **H**, b) NB7@**H**, c) NO7@**H**. [**H**] = [NB7] = [NO7] = 1 mmol/L. The red checkmark indicates the guest enters into the cavity of **H**.

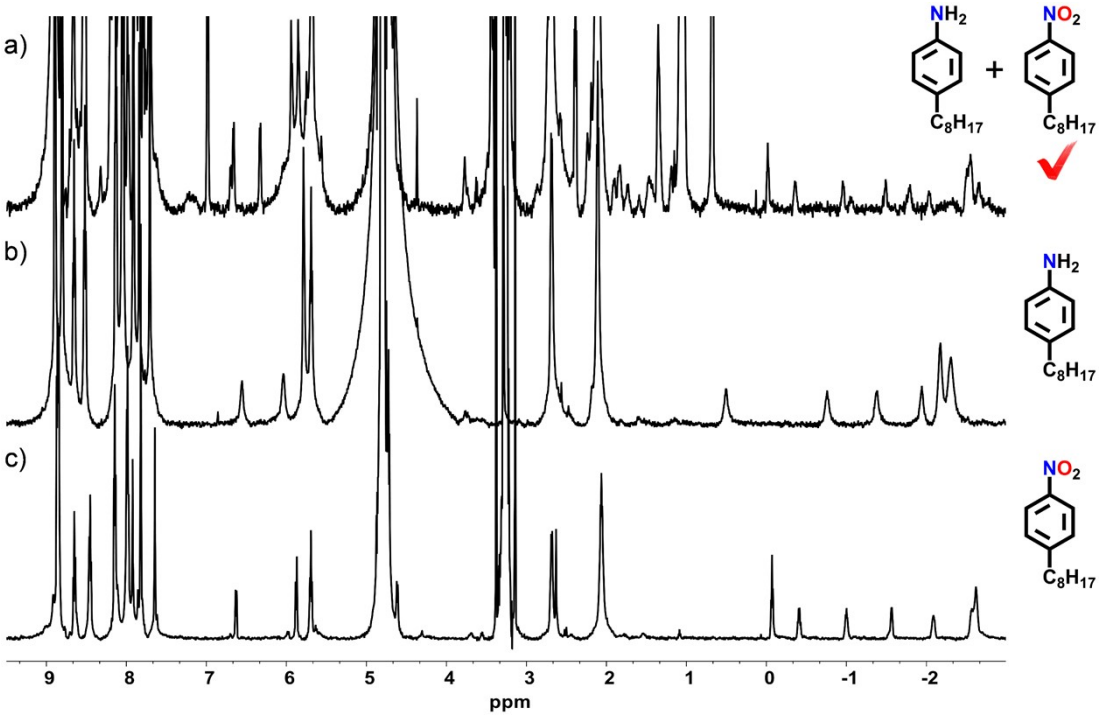

Fig. S34 ^{1}H NMR (600 MHz, D_2O, 298 K) spectra of a) NB8, NO8 and **H**, b) NB8@**H**, c) NO8@**H**. [**H**] = [NB8] = [NO8] = 1 mmol/L. The red checkmark indicates the guest enters into the cavity of **H**.

Based on the K_a value obtained from three independent experiments (Table S13), the c value was calculated to be 2.87. The titration curve exhibits a clear sigmoidal shape with an inflection point and a terminal plateau, the fit residuals are randomly distributed (within –1 to 5), and the RSD of K_a is 5.60%. Therefore, the binding constant for the NB6@**H** complex can be considered reliable.

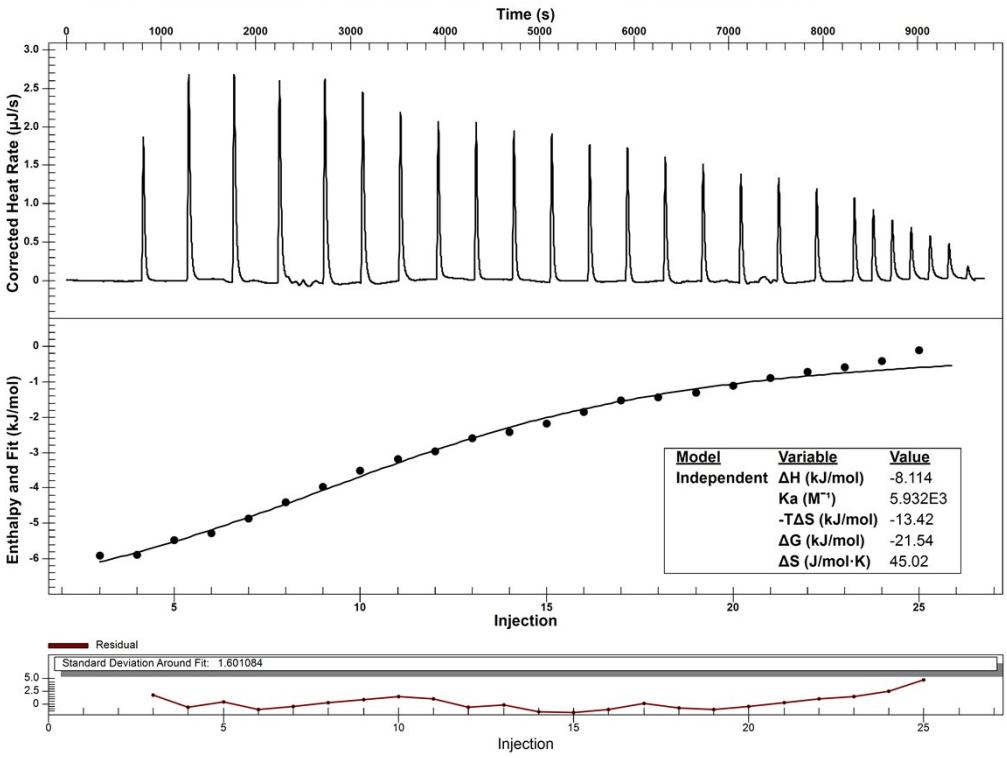

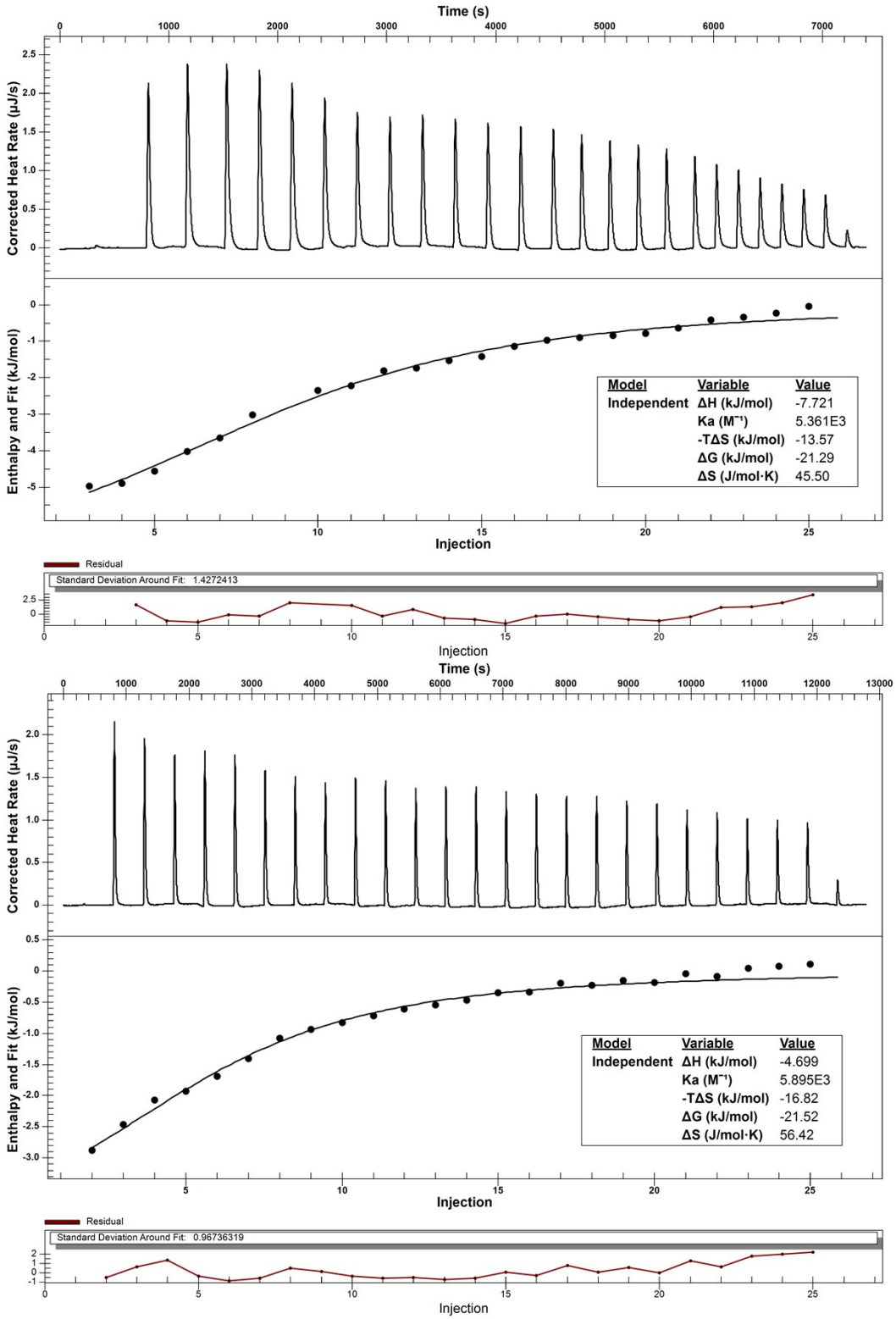

Fig. S35 Results from three independent ITC titrations of cavitand **H** (0.5 mmol/L) with NB6 (5 mmol/L) in 5% (v/v) MeOH/water. The raw titration curves (top), the corresponding reaction heat obtained from the integration of each injection peak (middle), and residual plot of the fit (bottom).

Table S13. Triplicate ITC data for the NB6@**H** complex

	1	2	3	Mean ± SD (K_a / M^{-1})	RSD / %
K (M^{-1})	5.93×10^3	5.36×10^3	5.90×10^3	$(5.73 \pm 0.32) \times 10^3$	5.60
ΔH (kJ/mol)	−8.11	−7.72	−4.70	−6.84 ± 1.87	27.3
ΔG (kJ/mol)	−21.54	−21.29	−21.52	−21.45 ± 0.14	0.65
ΔS (J/mol·K)	45.02	45.50	56.42	48.98 ± 6.45	13.2
Residual SD	1.60	1.43	0.97	-	-

Note: values are rounded to two decimal places

Based on the K_a value obtained from three independent experiments (Table S14), the c value was calculated to be 23.4. This value falls within the conventionally recommended range of 5-500, indicating favorable experimental conditions for reliable ITC fitting. The titration curve exhibits a clear sigmoidal shape with a distinct inflection point and a terminal plateau, the fit residuals are randomly distributed (within –2 to 2.5), and the RSD of K_a is 4.26%. Thus, the results are reliable.

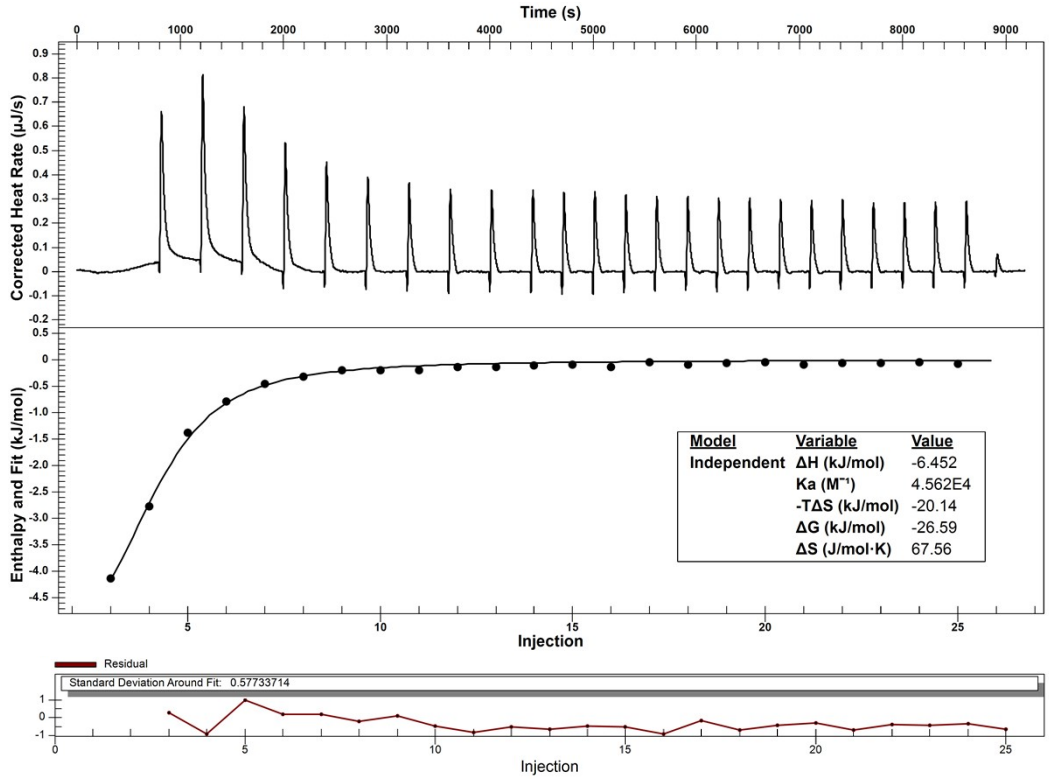

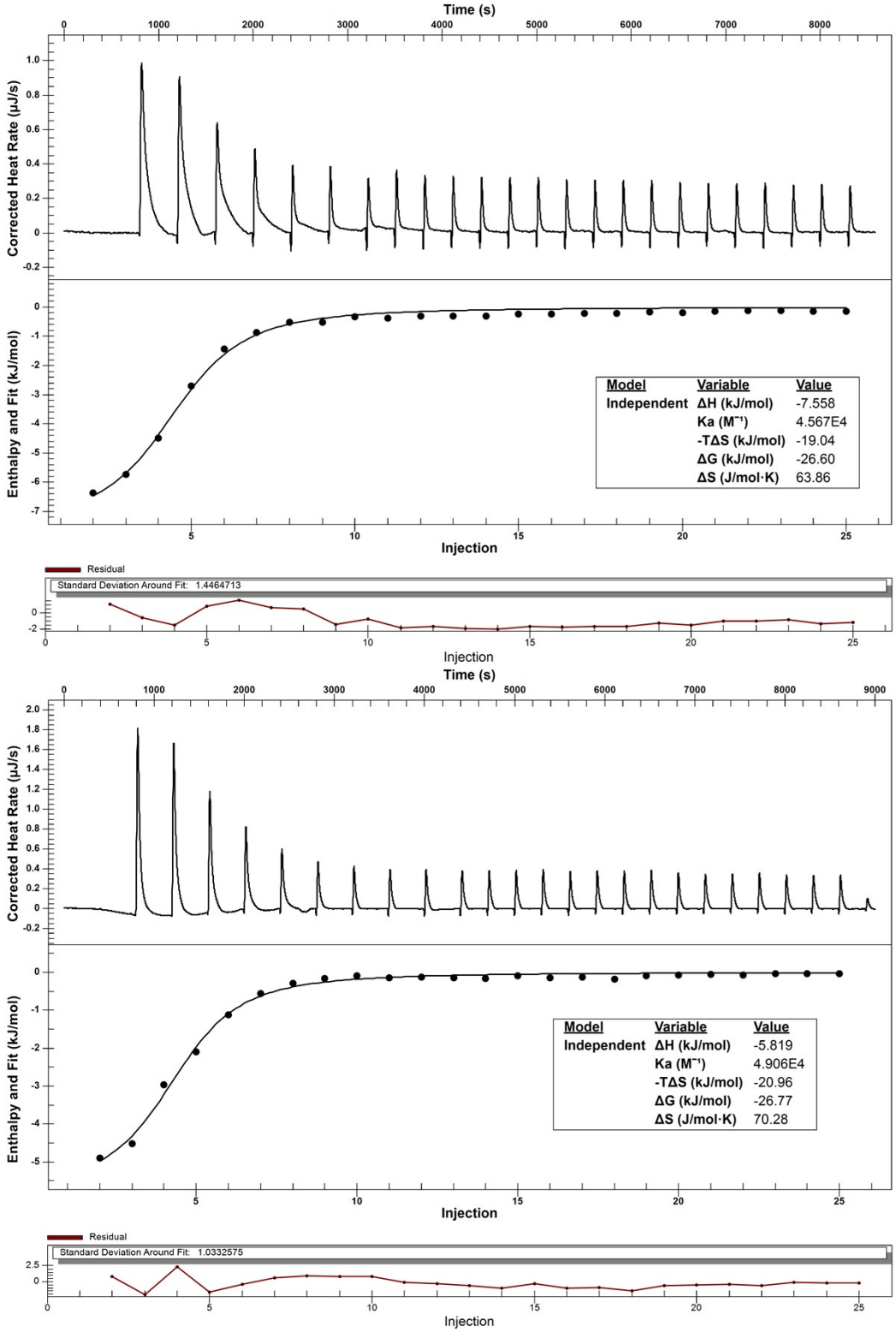

Fig. S36 Results from three independent ITC titrations of cavitand **H** (0.5 mmol/L) with NO6 (5 mmol/L) in 5% (v/v) MeOH/water. The raw titration curves (top), the corresponding reaction heat obtained from the integration of each injection peak (middle), and residual plot of the fit (bottom).

Table S14. Triplicate ITC data for the NO6@**H** complex

	1	2	3	Mean ± SD (K_a / M^{-1})	RSD / %
K (M^{-1})	4.56×10^4	4.57×10^4	4.91×10^4	$(4.68 \pm 0.20) \times 10^4$	4.26
ΔH (kJ/mol)	−6.45	−7.56	−5.82	−6.61 ± 0.88	13.3
ΔG (kJ/mol)	−26.59	−26.60	−26.77	−26.65 ± 0.10	0.38
ΔS (J/mol·K)	67.56	63.86	70.28	67.23 ± 3.22	4.79
Residual SD	0.58	1.45	1.03	-	-

Note: values are rounded to two decimal places

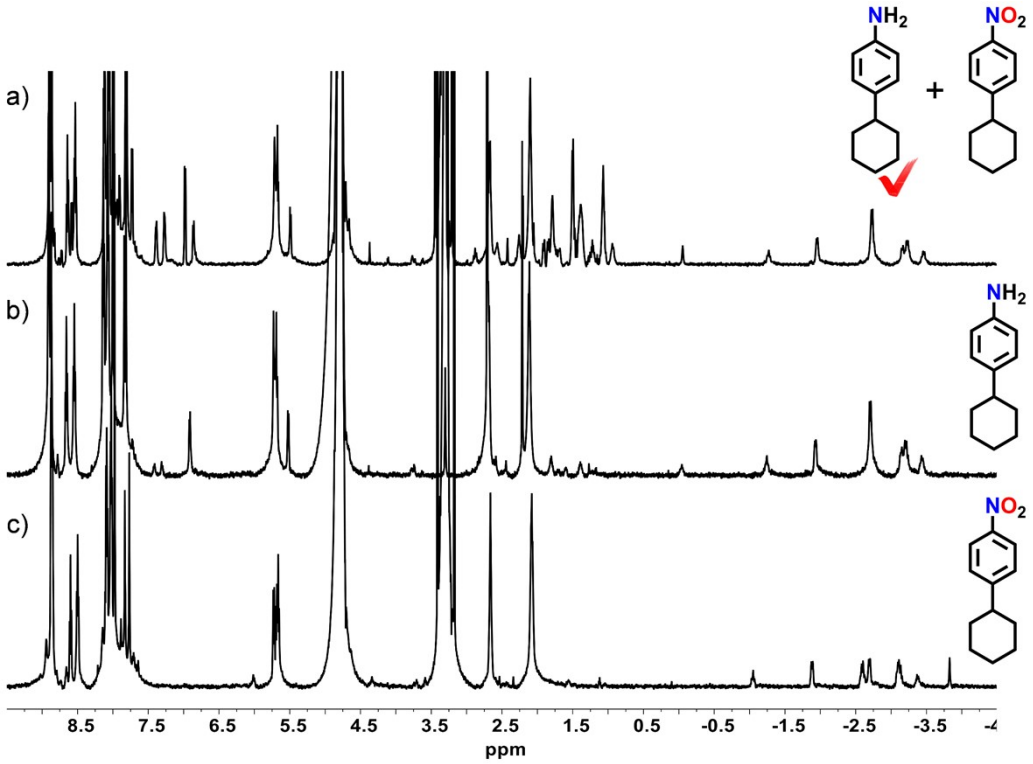

Fig. S37 ^{1}H NMR (600 MHz, D_2O, 298 K) spectra of a) 4-cyclohexylaniline, 4-cyclohexylnitrobenzene and **H**, b) 4-cyclohexylaniline@**H**, c) 4-cyclohexylnitrobenzene@**H**. [**H**] = [4-cyclohexylaniline] = [4-cyclohexylnitrobenzene] = 1 mmol/L. The red checkmark indicates the guest enters into the cavity of **H**.

Two independent competition experiments for 4-cyclohexylaniline vs. 4-cyclohexylnitrobenzene both show exclusive encapsulation of 4-cyclohexylaniline (Fig. S38), confirming the reproducibility of the selectivity.

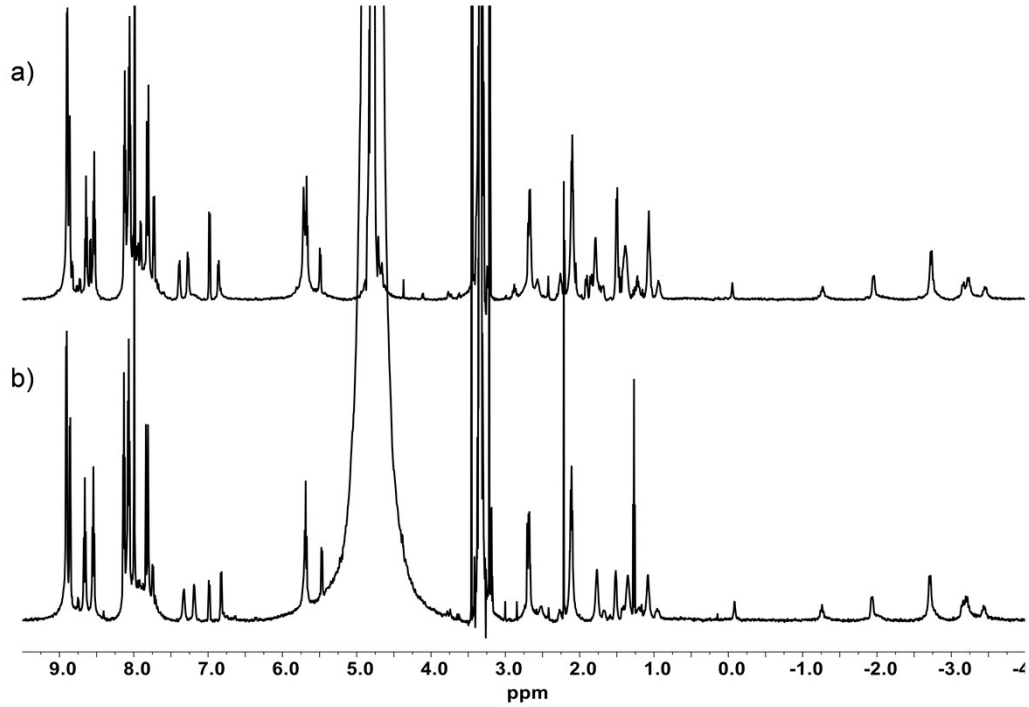

Fig. S38 ^{1}H NMR (600 MHz, D_2O, 298 K) spectra of two independent replicate competition experiments (a and b) of 4-cyclohexylaniline, 4-cyclohexylnitrobenzene and **H**. [**H**] = [4-cyclohexylaniline] = [4-cyclohexylnitrobenzene] = 1 mmol/L.

Based on the K_a value obtained from three independent experiments (Table S15), the c value was calculated to be 21.4. This value falls within the conventionally recommended range of 5-500, indicating favorable experimental conditions for reliable ITC fitting. The titration curve exhibits a clear sigmoidal shape with a distinct inflection point and a terminal plateau, the fit residuals are randomly distributed (within –1 to 1), and the RSD of K_a is 3.60%. Thus, the results are reliable.

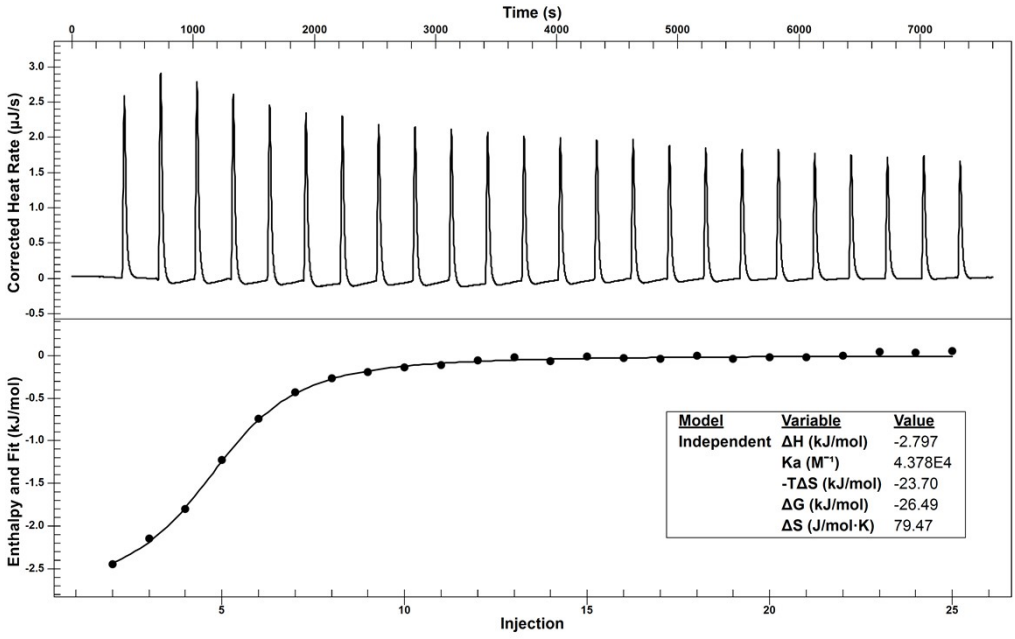

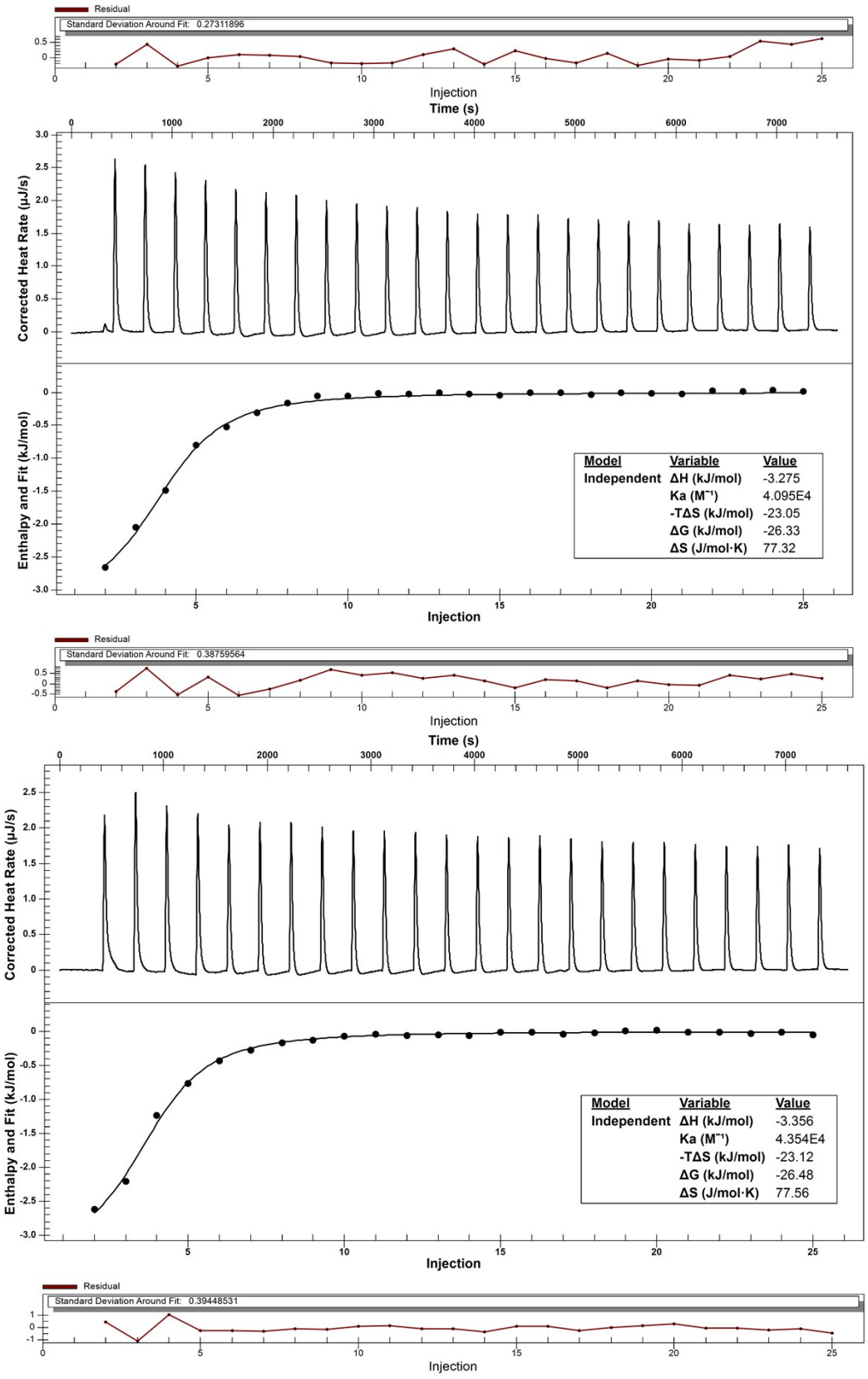

Fig. S39 Results from three independent ITC titrations of cavitand **H** (0.5 mmol/L) with 4-cyclohexylaniline (5 mmol/L) in 5% (v/v) MeOH/water. The raw titration curves (top), the corresponding reaction heat obtained from the integration of each injection peak (middle), and residual plot of the fit (bottom).

Table S15. Triplicate ITC data for the 4-cyclohexylaniline@**H** complex

	1	2	3	Mean ± SD	RSD / %
K (M^{-1})	4.38×10^4	4.10×10^4	4.35×10^4	$(4.28 \pm 0.15) \times 10^4$	3.60
ΔH (kJ/mol)	−2.80	−3.28	−3.36	−3.15 ± 0.31	9.90
ΔG (kJ/mol)	−26.49	−26.33	−26.48	−26.43 ± 0.09	0.34
ΔS (J/mol·K)	79.47	77.32	77.56	78.12 ± 1.18	1.51
Residual SD	0.27	0.39	0.39	-	-

Note: values are rounded to two decimal places

Based on the K_a value obtained from three independent experiments (Table S16), the c value was calculated to be 3.52. The titration curve exhibits a clear sigmoidal shape with an inflection point and a terminal plateau, the fit residuals are randomly distributed (within –1 to 1), and the RSD of K_a is 1.71%. Therefore, the binding constant for the 4-cyclohexylnitrobenzene@**H** complex can be considered reliable.

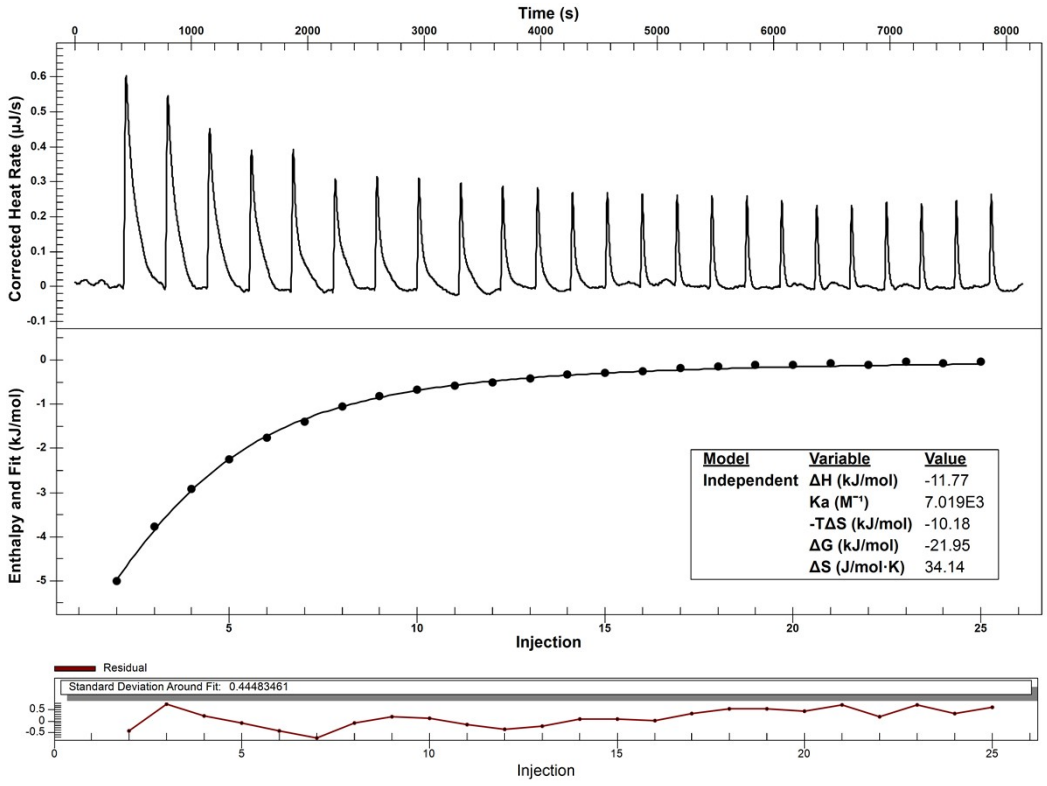

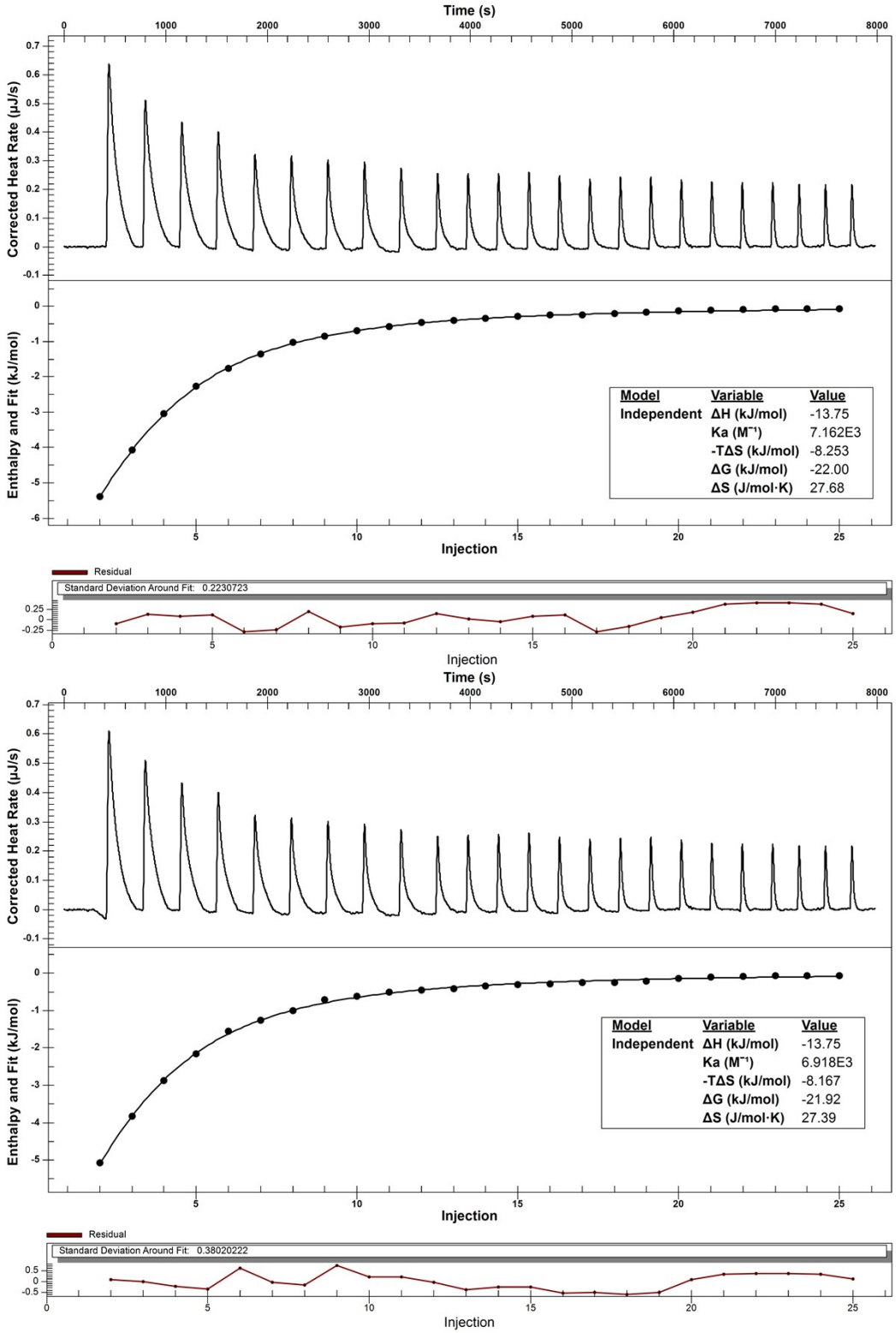

Fig. S40 Results from three independent ITC titrations of cavitand **H** (0.5 mmol/L) with 4-cyclohexylnitrobenzene (5 mmol/L) in 5% (v/v) MeOH/water. The raw titration curves (top), the corresponding reaction heat obtained from the integration of each injection peak (middle), and residual plot of the fit (bottom).

Table S16. Triplicate ITC data for the 4-cyclohexylnitrobenzene@**H** complex

	1	2	3	Mean ± SD (K_a / M^{-1})	RSD / %
K (M^{-1})	7.02×10^3	7.16×10^3	6.92×10^3	$(7.03 \pm 0.12) \times 10^3$	1.71
ΔH (kJ/mol)	−11.77	−13.75	−13.75	−13.09 ± 1.14	8.71
ΔG (kJ/mol)	−21.95	−22.00	−21.92	−21.96 ± 0.04	0.18
ΔS (J/mol·K)	34.14	27.68	27.39	29.74 ± 3.79	12.7
Residual SD	0.44	0.22	0.38	-	-

Note: values are rounded to two decimal places

6. Recognition behaviors of 4-alkylphenol and 4-alkylbenzoic acid by cavitand H

As shown in Fig. S41, for OH5-OH6, broadened complexation peaks were observed in the upfield region, indicating that the polar hydroxyl group led to a relatively fast rate of guest in-out from the cavity.[7-11] But for OH7 and OH8, the complexation peaks were sharper and more well-defined, indicating higher stability of the complexes formed. Based on the changes in the Δδ values of the alkyl protons (Table S17), it was determined that the terminal CH_3 group of OH5 was located deepest within the cavity, adopting an "extended" conformation. Meanwhile, the Δδ value of the OH_α proton on the phenol group was only −0.11 ppm, suggesting that the group was positioned relatively close to the cavity opening. For OH6-OH8, the Δδ value of the terminal CH_3 group was no longer the smallest, indicating "folded" conformations. Concurrently, the Δδ values of the OH_α proton varied within the range of −0.53 to −0.80 ppm, indicating that the phenol group had entered the cavity. This further drove the folding of the guest's alkyl tail. Additionally, the H_a and H_d protons on the upper rim of cavitand **H** also exhibited significant upfield shifts (Fig. S46a and Table S19).

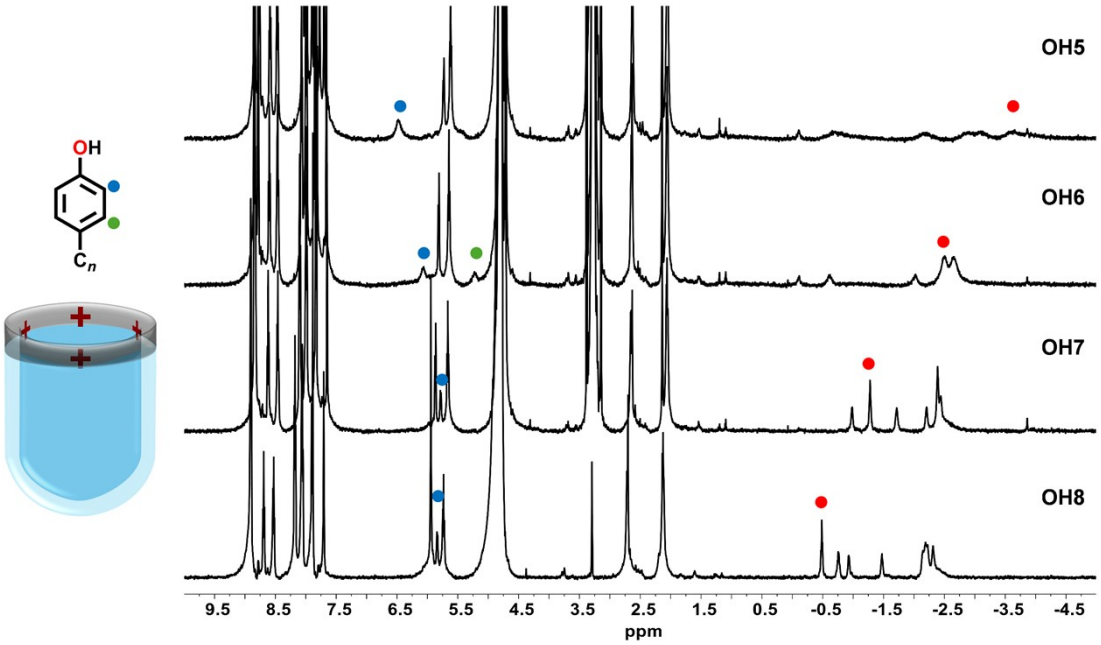

Fig. S41 ^{1}H NMR (600 MHz, D_2O, 298 K) spectra of **H** bound to 4-alkylphenol guests. The blue and green dots represent the positions of the α-CH protons (OH_α) and β-CH protons (OH_β) on the phenol group, respectively, and the red dots correspond to the terminal CH_3 groups of guests.

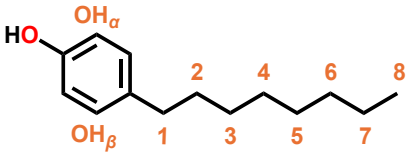

Fig. S42 The structure of OH8.

Table S17. Δδ values of alkyl chains for 4-alkylphenol guests upon bound to **H**

G@**H** / Δδ/ppm / C_n	OH5 @**H**	OH6 @**H**	OH7 @**H**	OH8 @**H**
OH_α	−0.11	−0.53	−0.80	−0.75
OH_β		−1.33		
1	−2.87	−2.81	−3.19	−2.96
2	−3.49	−3.30	−3.02	−2.77
3	−3.96	−3.69	−3.32	−3.26
4	−4.18	−3.69	−3.50	−3.30
5	−4.37	−3.77	−3.55	−3.43
6		−3.39	−3.50	−3.30
7			−2.01	−2.04
8				−1.21

For 4-alkylbenzoic acids, the $|\Delta\delta|$ values of the terminal CH_3 groups for all guests are smaller than those of the CH_2 groups, indicating that the alkyl chains adopt a folded conformation inside the cavity (Fig. S43 and Table S18). And the H_a and H_d protons on the upper rim of cavitand **H** also exhibited significant upfield shifts (Fig. S46b and Table S20).

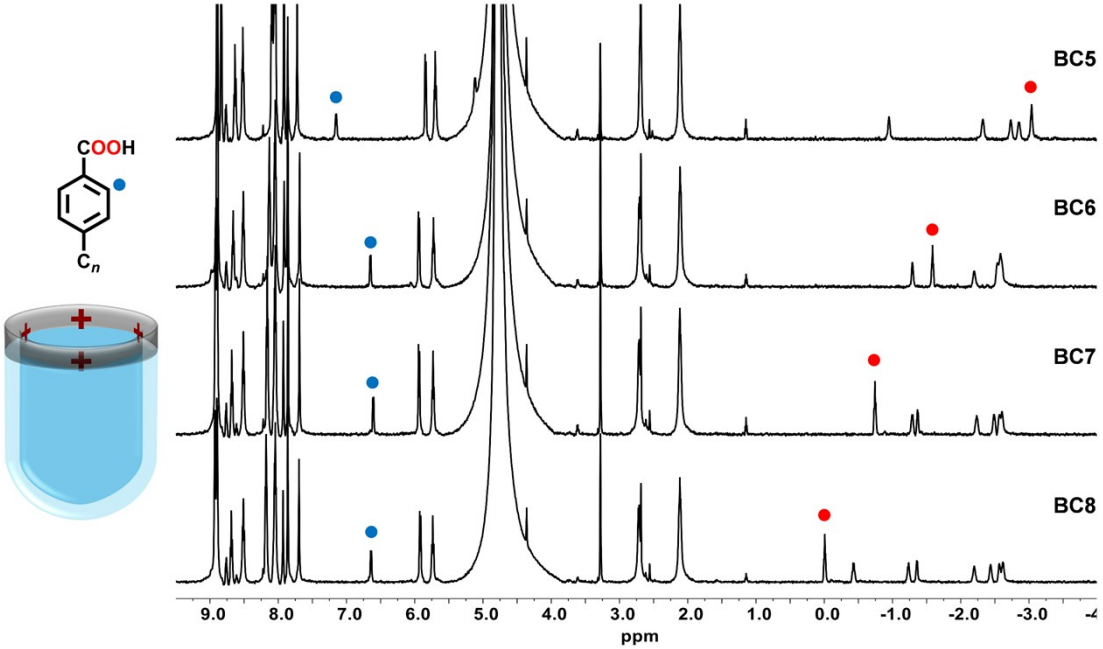

Fig. S43 ^{1}H NMR (600 MHz, D_2O, 298 K) spectra of **H** bound to 4-alkylbenzoic acid guests. The blue dots represent the positions of the α-CH protons (BC_α) on the benzoic acid group, and the red dots correspond to the terminal CH_3 groups of guests.

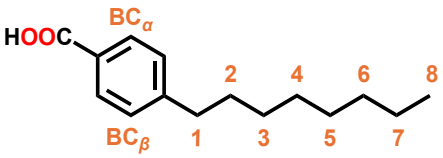

Fig. S44 The structure of BC8.

Table S18. Δδ values of alkyl chains for 4-alkylbenzoic acid guests upon bound to **H**

G@**H** / Δδ/ppm / C_n	BC5 @**H**	BC6 @**H**	BC7 @**H**	BC8 @**H**
BC_α	−0.61	−1.11	−1.16	−1.12
1	−3.59	−3.94	−3.93	−3.88
2	−3.92	−3.80	−3.82	−3.79
3	−4.01	−3.81	−3.84	−3.71
4	−4.09	−3.85	−3.87	−3.85
5	−3.85	−3.81	−3.72	−3.79
6		−2.40	−2.60	−2.59
7			−1.55	−1.65
8				−0.82

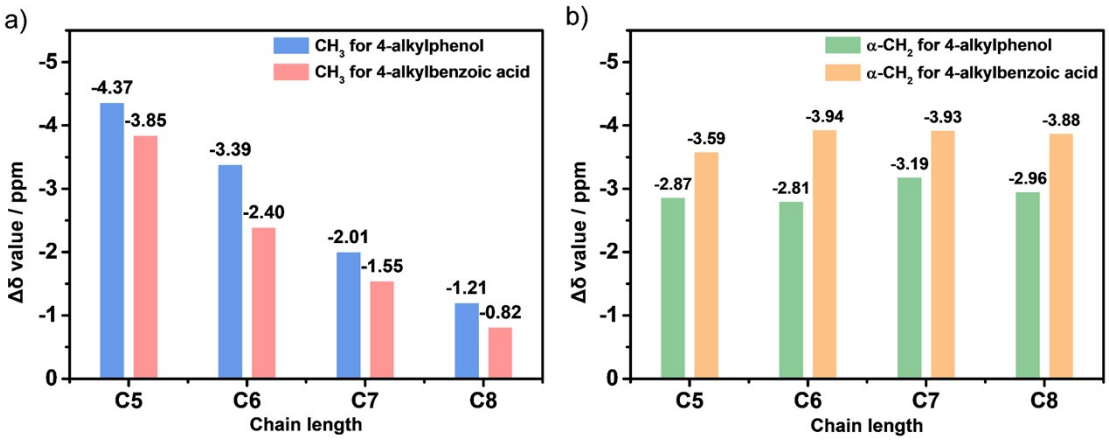

Fig. S45 Bar chart showing the variation of Δδ values for a) terminal CH_3 groups and b) α-CH_2 groups of 4-alkylphenols and 4-alkylbenzoic acids (n = 5-8) within **H**.

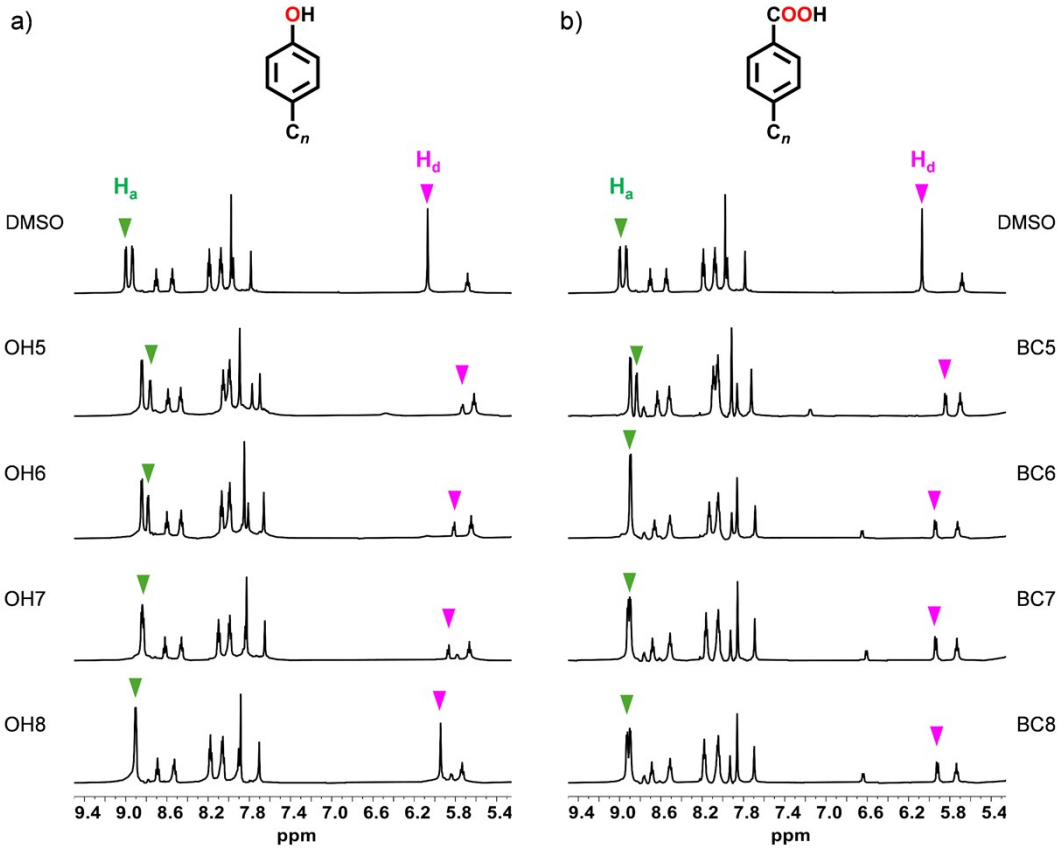

Fig. S46 Partial ^{1}H NMR (600 MHz, D_2O, 298 K) spectra (5.5 to 9.5 ppm) of **H** bound to a) 4-alkylphenol and b) 4-alkylbenzoic acid guests. The green and pink triangles indicate the H_a and H_d positions of **H** after bound to guests.

Table S19. The Δδ values for H_a and H_d of **H** bound to 4-alkylphenol guests

H@G / Δδ/ppm / C_n	**H**@OH5	**H**@OH6	**H**@OH7	**H**@OH8
H_a	−0.24	−0.22	−0.18	−0.10
H_d	−0.33	−0.26	−0.21	−0.13

Table S20. The Δδ values for H_a and H_d of **H** bound to 4-alkylbenzoic acid guests

H@G / Δδ/ppm / C_n	**H**@BC5	**H**@BC6	**H**@BC7	**H**@BC8
H_a	−0.17	−0.11	−0.08	−0.08
H_d	−0.22	−0.12	−0.12	−0.14

7. Competition experiments for 4-alkylphenol and 4-alkylbenzoic acid

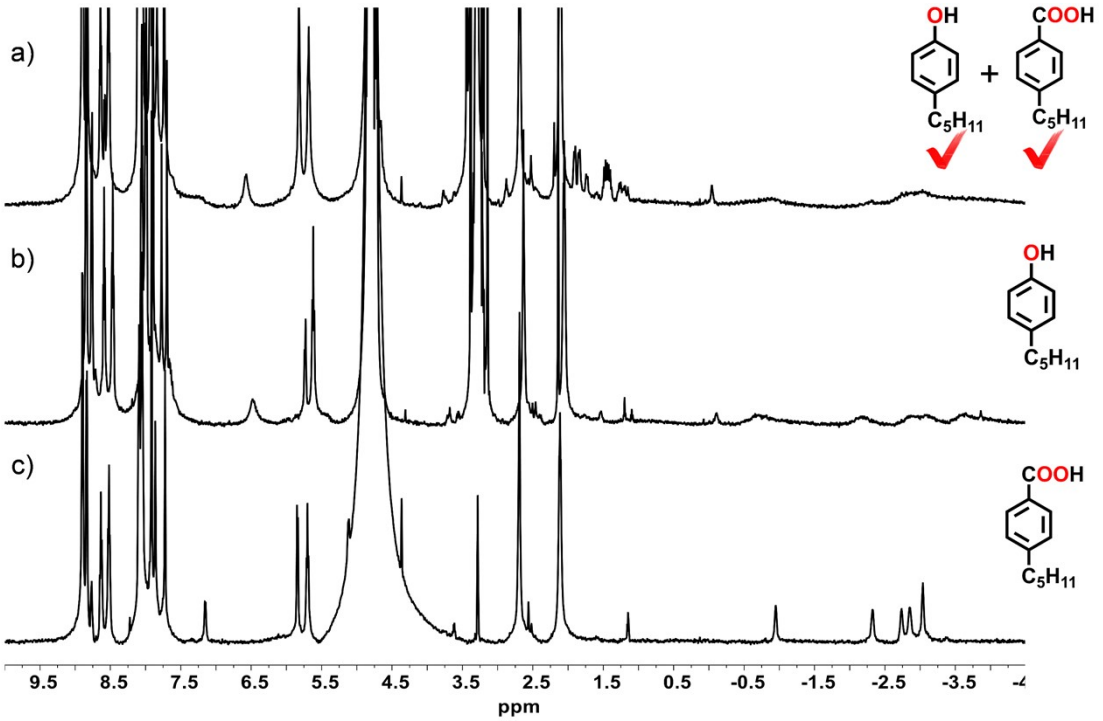

Fig. S47 ^{1}H NMR (600 MHz, D_2O, 298 K) spectra of a) OH5, BC5 and **H**, b) OH5@**H**, c) BC5@**H**. [**H**] = [OH5] = [BC5] = 1 mmol/L. The red checkmarks indicate the guests enter into the cavity of **H**.

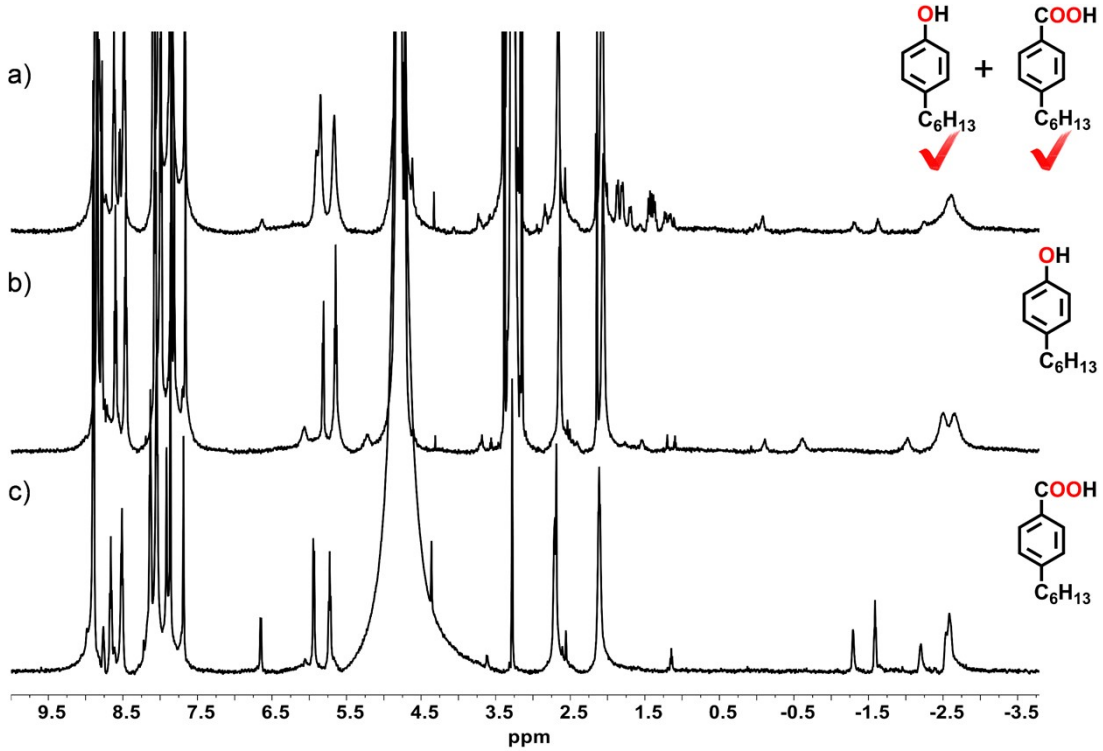

Fig. S48 ^{1}H NMR (600 MHz, D_2O, 298 K) spectra of a) OH6, BC6 and **H**, b) OH6@**H**, c) BC6@**H**. [**H**] = [OH6] = [BC6] = 1 mmol/L. The red checkmarks indicate the guests enter into the cavity of **H**.

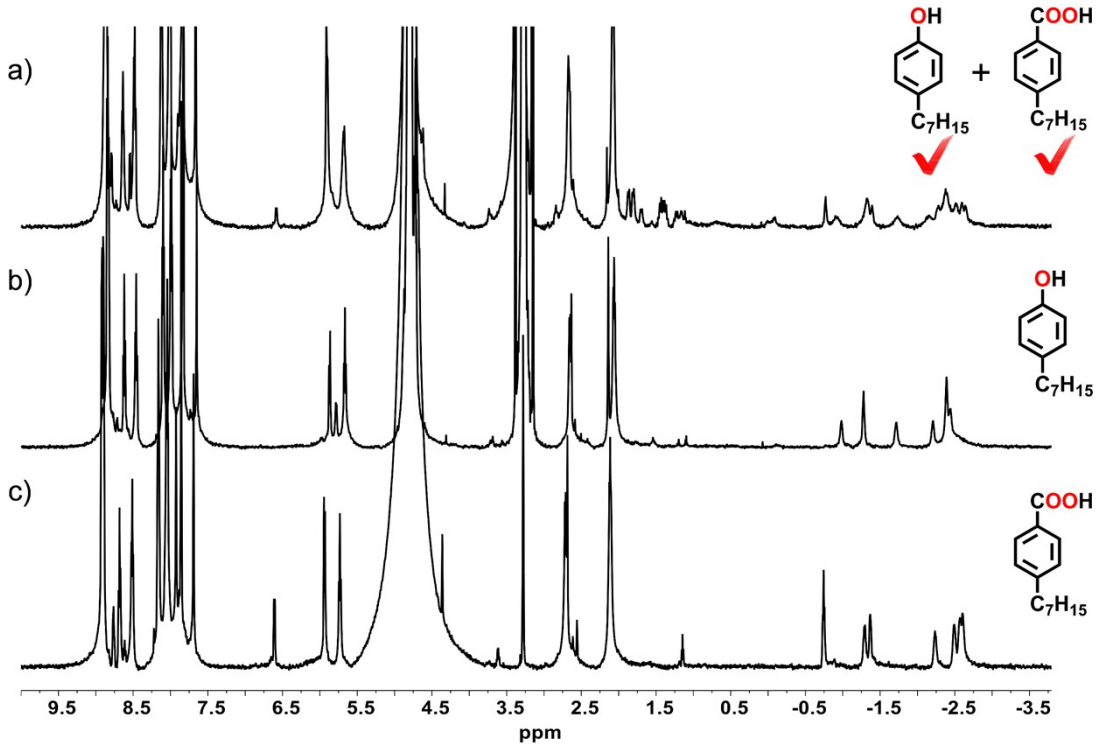

Fig. S49 ^{1}H NMR (600 MHz, D_2O, 298 K) spectra of a) OH7, BC7 and **H**, b) OH7@**H**, c) BC7@**H**. [**H**] = [OH7] = [BC7] = 1 mmol/L. The red checkmarks indicate the guests enter into the cavity of **H**.

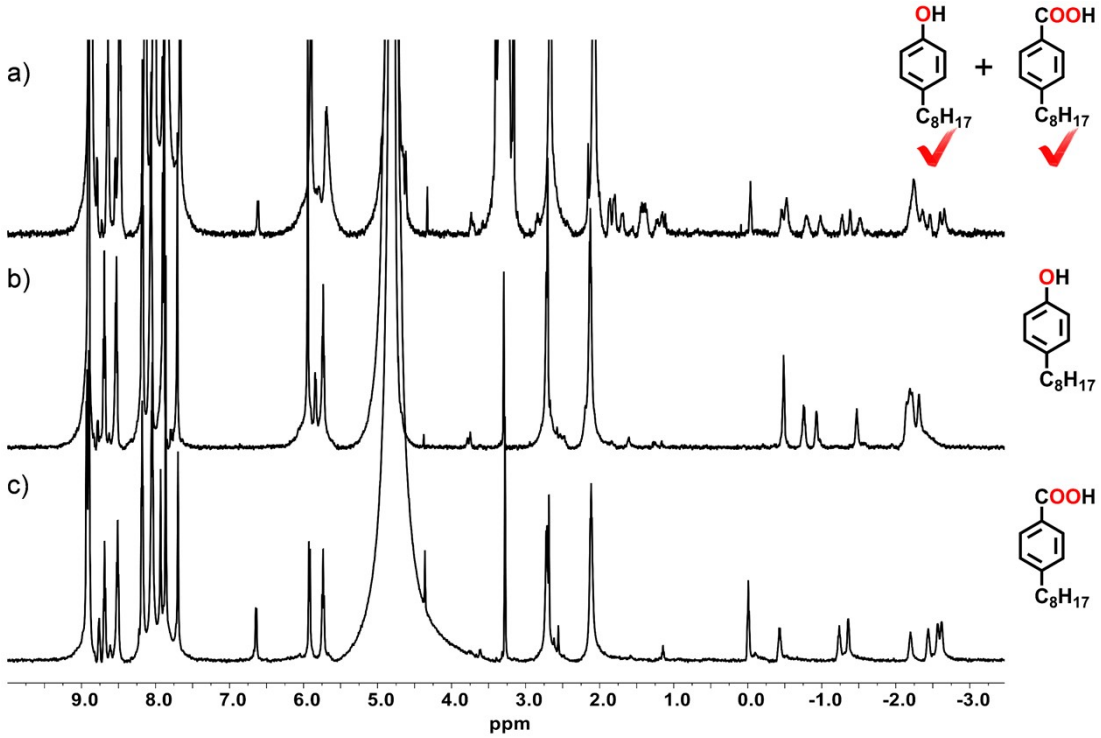

Fig. S50 ^{1}H NMR (600 MHz, D_2O, 298 K) spectra of a) OH8, BC8 and **H**, b) OH8@**H**, c) BC8@**H**. [**H**] = [OH8] = [BC8] = 1 mmol/L. The red checkmarks indicate the guests enter into the cavity of **H**.

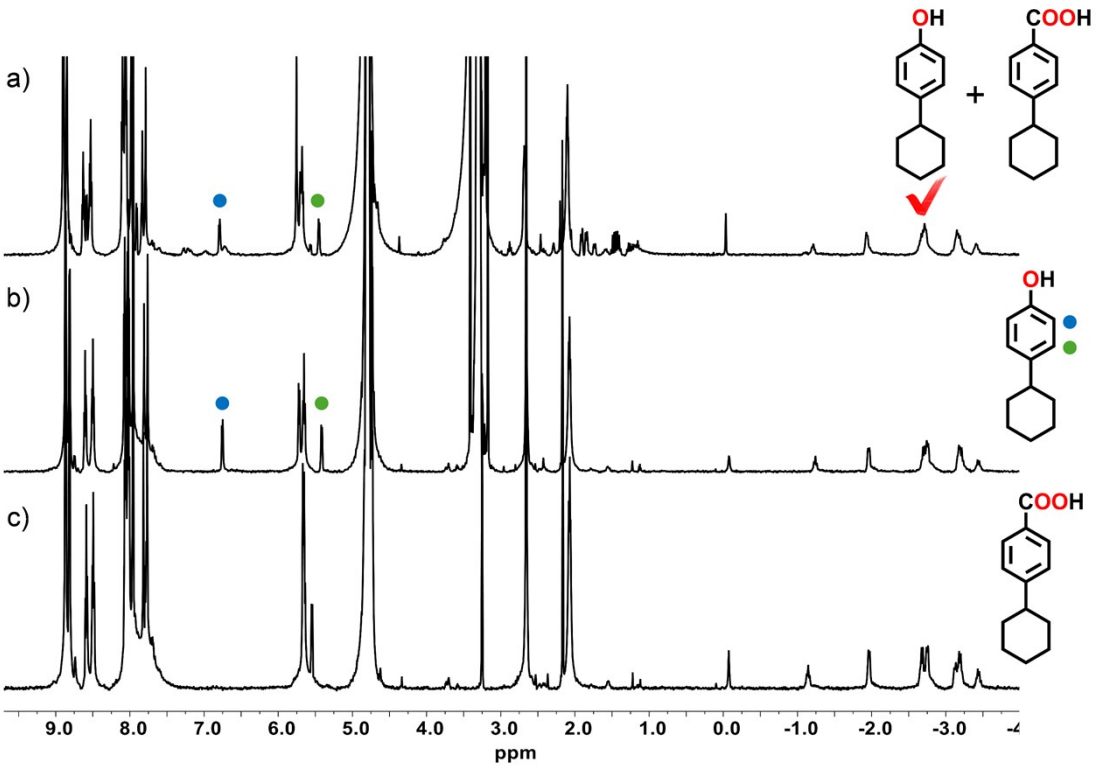

Fig. S51. ^{1}H NMR (600 MHz, D_2O, 298 K) spectra of a) 4-cyclohexylphenol, 4-cyclohexylbenzoic acid and **H**, b) 4-cyclohexylphenol@**H**, c) 4-cyclohexylbenzoic acid@**H**. [**H**] = [4-cyclohexylphenol] = [4-cyclohexylbenzoic acid] = 1 mmol/L. The blue and green dots represent the positions of the α-CH and β-CH proton on the phenol group, respectively. The red checkmark indicates the guest enters into the cavity of **H**.

8. References

1. Q. Wang, Y. Chen, M. Zhao, W. Yang, J. Rebek and Y. Yu, *Chin. Chem. Lett.*, in press (DOI: 10.1016/j.cclet.2026.112889).

2. M. Tang, K. Kanagaraj, J. Rebek and Y. Yu, *Chem.-Asian J.*, 2022, **17**, e202200466.

3. M. Kaur, J. C. Cooper and J. F. V. Humbeck, *Org. Biomol. Chem.*, 2024, **22**, 4888–4894.

4. T. Wiseman, S. Williston, J. F. Brandts and L.-N. Lin, *Anal. Biochem.*, 1989, **179**, 131–137.

5. W. B. Turnbull and A. H. Daranas, *J. Am. Chem. Soc.*, 2003, **125**, 14859–14866.

6. J. Chen, W. Tian, Y. Yun, Y. Tian, C. Sun, R. Ding and H. Chen, *Arch. Biochem. Biophys.*, 2021, **713**, 109045.

7. J. I. Kaplan, *Phys. Rev. A*, 1980, **22**, 1022–1024.

8. A. Shivanyuk and J. Rebek, *Chem. Commun.*, 2002, 2326–2327.

9. A. Scarso, L. Trembleau and J. Rebek, *J. Am. Chem. Soc.*, 2004, **126**, 13512–13518.

10. V. Březina, L. Hanyková, N. Velychkivska, J. P. Hill and J. Labuta, *Sci. Rep.*, 2022, **12**, 17369.

11. L. Perez, B. G. Caulkins, M. Mettry, L. J. Muellera and R. J. Hooley, *Chem. Sci.*, 2018, **9**, 1836–1845.